

1 **mGluR7 allosteric modulator AMN082 corrects protein**
2 **synthesis and pathological phenotypes in FXS**

3
4
5 Vipendra Kumar¹, Kwan Young Lee¹, Anirudh Acharya¹, Matthew S Babik¹, Catherine A
6 Christian-Hinman^{1,2,3}, Justin S Rhodes^{2,3,4} and Nien-Pei Tsai^{1,2,3*}

7
8
9 ¹Department of Molecular and Integrative Physiology, School of Molecular and Cellular Biology,
10 University of Illinois at Urbana-Champaign, Urbana, IL 61801, USA

11 ²Neuroscience Program, University of Illinois at Urbana-Champaign, Urbana, IL 61801, USA

12 ³Beckman Institute for Advanced Science and Technology, University of Illinois at Urbana-
13 Champaign, Urbana, IL 61801, USA

14 ⁴Department of Psychology, University of Illinois at Urbana-Champaign, Champaign, IL 61820,
15 USA

16
17 *Correspondence: Nien-Pei Tsai, Ph.D.

18 407 South Goodwin Ave., Urbana, IL 61801, USA

19 Tel: 217-244-5620 Fax: 217-333-1133

20 Email: nptsai@illinois.edu

21 ORCID: 0000-0003-1032-0107

22
23 Running title: mGluR7 and FXS
24
25
26
27
28
29

30 **SUMMARY**

31 Fragile X syndrome (FXS) is the leading cause of inherited autism and intellectual
32 disabilities. Aberrant protein synthesis due to the loss of fragile X messenger ribonucleoprotein
33 (FMRP) is the major defect in FXS, leading to a plethora of cellular and behavioral abnormalities.
34 However, no treatments are available to date. In this study, we found that activation of
35 metabotropic glutamate receptor 7 (mGluR7) using a positive allosteric modulator named
36 AMN082 represses protein synthesis through ERK1/2 and eIF4E signaling in an FMRP-
37 independent manner. We further demonstrated that treatment of AMN082 leads to a reduction in
38 neuronal excitability, which in turn ameliorates audiogenic seizure susceptibility in *Fmr1* KO
39 mice, the FXS mouse model. When evaluating the animals' behavior, we showed that treatment
40 of AMN082 reduces repetitive behavior and improves learning and memory in *Fmr1* KO mice.
41 This study uncovers novel functions of mGluR7 and AMN082 and suggests the activation of
42 mGluR7 as a potential therapeutic approach for treating FXS.

43

44

45 **KEY WORDS**

46 FXS, FMRP, mGluR7, autism, protein synthesis

47

48

49

50

51 INTRODUCTION

52 Fragile X syndrome (FXS) is monogenic and inherited and is the most prevalent form of
53 autism. It affects 1:4000 males and 1:8000 females (Hagerman *et al*, 2009; Budimirovic &
54 Kaufmann, 2011; Turner *et al*, 1996). Major clinical symptoms of FXS involve intellectual
55 disability, hyperarousal, hyperactivity, and seizures (Hagerman *et al*, 2017; Hagerman &
56 Hagerman, 2022; Berry-Kravis *et al*, 2010). FXS is caused by the lack of fragile X messenger
57 ribonucleoprotein (FMRP) that is encoded by the *Fmr1* gene. In FXS, the *Fmr1* gene is
58 transcriptionally silenced due to abnormally expanded CGG repeats (> 200) that lead to DNA
59 hypermethylation. FMRP is primarily involved in repression of protein synthesis by directly or
60 indirectly interfering with translating mRNAs (Hagerman & Hagerman, 2022). A growing body
61 of evidence arising from various model systems of FXS has confirmed that exaggerated protein
62 synthesis is central to most disease-specific molecular and behavioral abnormalities in FXS
63 (Bolduc *et al*, 2008; Till *et al*, 2015; Bhakar *et al*, 2012; Osterweil *et al*, 2010; Raj *et al*, 2021).
64 Many strategies aimed at rebalancing basally elevated protein synthesis in FXS have been
65 introduced (Dölen & Bear, 2008; Michalon *et al*, 2012; Sharma *et al*, 2010; Gurney *et al*, 2017;
66 McCamphill *et al*, 2020). Among them, inhibition of metabotropic glutamate receptor 5
67 (mGluR5) is most extensively studied as multiple mGluR5 antagonists have been shown to
68 exhibit disease-modifying potential by causing a reduction in protein synthesis and correction in
69 behavioral abnormalities in FXS animal models, such as *Fmr1* KO mice. However, the
70 unfortunate failure of clinical trials, such as the one for the negative allosteric modulator (NAM)
71 against mGluR5, Mavoglurant (Scharf *et al*, 2015; Berry-Kravis *et al*, 2016), has prompted the
72 search for alternative therapeutic strategies.

73 mGluR7, an understudied mGluR, belongs to group III mGluRs along with other
74 members, namely mGluR4, mGluR6, and mGluR8. Although group III mGluRs have been
75 shown to participate in synaptic plasticity via ERK/MAPK signaling (Dasgupta *et al*, 2020), the
76 detailed function and mechanism of individual group III mGluRs remain unclear. Subcellular
77 localization studies have shown that mGluR7 can be located in the presynaptic active zones of
78 glutamatergic and GABAergic neurons in somatosensory cortex and hippocampus (Shigemoto *et*
79 *al*, 1997; Dalezios *et al*, 2002) as well as postsynaptic membranes of glutamatergic neurons in
80 the prefrontal cortex (Gu *et al*, 2012). mGluR7 is encoded by *Grm7* gene, a known autism-linked
81 gene whose truncation and missense mutations have been associated with idiopathic autism and
82 developmental delay (Yang & Pan, 2013; Fisher *et al*, 2018). Studies have demonstrated that
83 mGluR7 can function by causing a decrease in excitatory neurotransmission through inhibition
84 of glutamate release from the presynaptic terminal (Palazzo *et al*, 2016). Based on this logic,
85 other studies have also shown that mice deficient in mGluR7 (*mGluR7* knockout [KO]) exhibit
86 increased seizure susceptibility (Sansig *et al*, 2001). Additionally, *mGluR7* KO mice also show
87 deficits in neuronal plasticity and working memory (Hölscher *et al*, 2005). Despite these prior
88 studies, the molecular mechanism by which mGluR7 achieves its physiological functions and
89 whether activation of mGluR7 can be a potential therapeutic approach for neurodevelopmental
90 disorders, such as FXS, remains unclear.

91 In this study, we showed that activation of mGluR7 using a positive allosteric modulator,
92 N,N'-dibenzhydrylethane-1,2-diamine, AMN082, causes a reduction in protein synthesis via
93 extracellular signal-regulated kinase 1/2- and eukaryotic translation initiation factor 4E (ERK1/2
94 and eIF4E, respectively)-associated signaling in an *Fmr1*-independent manner. Furthermore, we
95 found that activation of mGluR7 leads to a significant reduction in neuronal excitability and

96 audiogenic seizure (AGS) phenotype in *Fmr1* KO mice. Additionally, mGluR7 activation by
97 AMN082 leads to a significant reduction in repetitive behavior and improvement in learning and
98 memory in *Fmr1* KO mice. Together, these findings reveal a novel mechanism underlying the
99 physiological effects of mGluR7 through translational control and suggest activation of mGluR7
100 as a potential therapeutic approach for treating FXS.

101

102 **RESULTS**

103 **Activation of mGluR7 reduces protein synthesis in both WT and *Fmr1* KO neurons.**

104 mGluR7 is highly expressed in multiple brain regions, including hippocampus, neocortex,
105 and hypothalamus (Kinzie *et al*, 1995; Bradley *et al*, 1996; Ohishi *et al*, 1995). To begin, we first
106 aimed to characterize the expression levels and patterns of mGluR7 between WT and *Fmr1* KO
107 mice. We performed immunohistochemical staining of mGluR7 using an antibody against
108 mGluR7a on brain sections from post-natal (P) day-60 male WT and *Fmr1* KO mice. No
109 commercially antibodies suitable for immunohistochemical staining are available against
110 mGluR7b, the other major isoform of mGluR7. As shown in Fig. 1A, we did not observe any
111 visible change in mGluR7a in the sub-regions of the hippocampus, including CA3, CA1, and
112 dentate gyrus between WT and *Fmr1* KO mice. Antibody specificity was confirmed using brain
113 sections from *mGluR7* KO mice. We next measured the expression of mGluR7a and mGluR7b in
114 the forebrain lysates of WT and *Fmr1* KO mice by western blotting. As shown in Fig. 1B,
115 consistent with our observation using brain sections, we did not find any significant changes in
116 the total levels of mGluR7a or mGluR7b between WT and *Fmr1* KO mice. Interestingly, when
117 performing surface protein biotinylation in WT and *Fmr1* KO primary cortical neuron cultures

118 followed by western blotting, we observed a slight but significant decrease in surface mGluR7a
119 but an increase in surface mGluR7b in *Fmr1* KO neurons when compared with WT neurons (Fig.
120 1C). It should be noted that cortical neurons were used to obtain enough cells for surface
121 biotinylation. Together, these data suggest a slight alteration of surface expression of mGluR7
122 isoforms in *Fmr1* KO neurons.

123 To begin exploring the effect of mGluR7 on protein synthesis, we treated WT and *Fmr1*
124 KO cortical neurons with a selective mGluR7 allosteric agonist, AMN082 (1 μ M) or antagonist
125 6-(4-Methoxyphenyl)-5-methyl-3-(4-pyridinyl)-isoxazolo[4,5-c]pyridin-4(5H)-one (MMPIP, 1
126 μ M) for 2 h and employed the surface sensing of translation (SUnSET) technique to label newly
127 synthesized protein with puromycin (10 μ g/ml) during the last hour of treatment. Puromycin-
128 labeled proteins were detected by western blotting using an anti-puromycin antibody. As shown
129 in Fig. 1D, we observed a significant increase in the protein synthesis in *Fmr1* KO neurons
130 compared to WT neurons, as has been observed previously (Dölen *et al*, 2007). Treatment of
131 AMN082 was able to cause significant reduction in protein synthesis in *Fmr1* KO cultures to a
132 level similar to basal WT levels. Because AMN082 treatment also significantly reduces protein
133 synthesis in WT cultures, it suggests that AMN082 acts through *Fmr1*-independent mechanism
134 in this novel translational control. The specificity of AMN082 to mGluR7 was confirmed using
135 cultures made from mGluR7 KO mice as no significant effects on protein synthesis were
136 observed (Fig. 1E). Interestingly, MMPIP does not have any effects on protein synthesis,
137 suggesting the possibility that basal mGluR7 activity might be low in cultured neurons. Because
138 *mGluR7* KO mainly impacts the expression of mGluR7a isoform (Fig. 1E), our results suggest
139 that activation of mGluR7, at least through mGluR7a, leads to *Fmr1*-independent repression of
140 protein synthesis.

141

142 **Activation of mGluR7 represses protein synthesis via ERK1/2 and eIF4E signaling.**

143 We next sought to understand the signaling pathway by which activation of mGluR7
144 represses protein synthesis. It is known that mGluR7 is coupled with inhibitory G-protein (G_i)
145 whose activation inhibits adenylyl cyclase and reduces cytosolic cAMP levels (Mitsukawa *et al*,
146 2005). We investigated two main regulators of activity-dependent protein synthesis in neurons
147 that are influenced by the changes in cytosolic cAMP levels: (1) ERK1/2 and (2) mammalian
148 target of rapamycin (mTOR) (Xie *et al*, 2011; Kim *et al*, 2010) To test whether one or both
149 proteins are involved, we treated WT and *Fmr1* KO cortical neuron cultures at days-in-vitro
150 (DIV) 14 with AMN082 (1 μ M) for 2 h and then measured the levels of phosphorylated ERK1/2
151 (Fig. 1F) and phosphorylated mTOR (Fig. 1G) by western blotting. As shown, we observed
152 significantly reduced levels of phosphorylated ERK1/2, but not phosphorylated mTOR, in both
153 WT and *Fmr1* KO neurons.

154 It has been shown that phosphorylated ERK1/2 interacts with and phosphorylates
155 mitogen-activated protein kinases-interacting kinases 1/2 (MNK1/2), which subsequently
156 phosphorylates eukaryotic translation initiation factor 4E (eIF4E), leading to facilitated
157 translation initiation (Waskiewicz *et al*, 1997; Pyronnet *et al*, 1999; Joshi *et al*, 1995) A recent
158 study suggested that inhibition of ERK1/2 causes significant upregulation in phosphorylation of
159 eukaryotic initiation factor 2-alpha (eIF2 α) and inhibits cap-dependent and -independent
160 translation (Parveen *et al*, 2021). To determine whether eIF4E, eIF2 α , or both are impacted
161 following activation of mGluR7, we measured the phosphorylation of eIF4E at Ser-209 and
162 eIF2 α at Ser-51 in WT and *Fmr1* KO cortical neuron cultures after treatment of AMN082 for 2 h.
163 As shown, we found that eIF4E phosphorylation was significantly reduced (Fig. 1H), while

164 eIF2 α phosphorylation was not altered (Fig. 1I) after treatments with AMN082 in both WT and
165 *Fmr1* KO neurons. Although we did not observe basally elevated eIF4E phosphorylation in
166 *Fmr1* KO cultures, which is known to be a brain region- and age-dependent effect (Liu *et al*,
167 2022), our data suggest that AMN082 represses protein synthesis through eIF4E phosphorylation.
168 To further test the suppressive effect of AMN082 on eIF4E, we measured the ability of eIF4E to
169 bind to the scaffolding protein eIF4G in cap-dependent translation initiation. To this end, we
170 assessed eIF4E-eIF4G complex by m7GTP pull-down assay, as performed previously (Santini *et*
171 *al*, 2017), in WT and *Fmr1* KO neuronal cultures treated with DMSO or AMN082. As shown
172 (Fig. 1J), both WT and *Fmr1* KO cultures treated with AMN082 showed a significant decrease
173 in the eIF4E-eIF4G interaction. These results confirmed the repressive effect of AMN082 on
174 eIF4E signaling.

175 To validate our observation *in vivo*, we intraperitoneally injected male WT and *Fmr1* KO
176 mice at 6-8 weeks of age with AMN082 (1 mg/kg) and puromycin (200 mg/kg) for one hour to
177 assess protein synthesis in the hippocampus. AMN082 is known to rapidly cross the blood-brain
178 barrier (Mitsukawa *et al*, 2005). As shown (Fig. 2A), we observed a significant increase in
179 protein synthesis in saline-treated *Fmr1* KO mice when compared to saline-treated WT mice,
180 suggesting increased protein synthesis in the hippocampus of *Fmr1* KO mice. Importantly,
181 treatment of AMN082 reduced protein synthesis in both WT and *Fmr1* KO mice, similar to what
182 we observed in cultured neurons (Fig. 1D). These effects on protein synthesis can also be seen
183 when we tested one of FMRP's target genes, protocadherin-7 (*Pcdh7*) in the hippocampus of WT
184 or *Fmr1* KO mice injected with saline or AMN082 (Fig. EV1). The specificity of AMN082 to
185 mGluR7 was confirmed as no significant effect was observed in *mGluR7* KO mice (Fig. 2B). We
186 further tested ERK1/2 and eIF4E signaling *in vivo* and confirmed a decrease in phosphorylated

187 ERK1/2 and eIF4E in both WT and *Fmr1* KO mice treated with AMN082 (1 mg/kg) (Figs. 2C
188 and 2D). Taken together, our results suggest that mGluR7 potentially acts through ERK1/2 and
189 eIF4E to repress protein synthesis (Figure 2E).

190

191 **Activation of mGluR7 reduces neuronal excitability.**

192 Activation of mGluR7 is known to lead to a reduction in presynaptic glutamate release
193 via inhibition of P/Q-type Ca²⁺ channels (Martín *et al*, 2007) and reduction in neuronal
194 excitability via inhibition of N-type calcium channels (Millán *et al*, 2002). However, it is unclear
195 whether mGluR7 activation is capable of attenuating pathological hyperexcitability, which is one
196 of the key neuronal abnormalities in FXS. To begin testing this possibility, we first tested the
197 effect of AMN082 on neuronal network activity using a multielectrode array (MEA) recording
198 system (Maestro Edge, Axion Biosystems). We treated WT and *Fmr1* KO neurons with dimethyl
199 sulfoxide (DMSO), AMN082 (1 μM), or the selective mGluR7 antagonist, MMPIP (1 μM) for 2
200 h and compared network activity pre- and post-treatment. As shown in Fig. 3A, a drastic
201 reduction in network activity can be seen with a corresponding reduction in spontaneous spike
202 rate, burst duration, and burst frequency in both WT and *Fmr1* KO cultures. In a manner similar
203 to that observed regarding protein synthesis (Fig. 1D), MMPIP did not elicit any significant
204 effects on network activity in either WT or *Fmr1* KO cultures.

205 The findings from the MEA recordings prompted us to evaluate the effect of mGluR7
206 activation at a single cell level. We performed whole-cell patch-clamp recording in WT and
207 *Fmr1* KO cortical neurons at DIV 14. We used a current-clamp recording to measure the action
208 potential firing rate after delivering constant somatic current pulses for durations of 500 ms in

209 the range of 0 to 200 pA (Liu *et al*, 2021). As anticipated, mGluR7 activation caused a
210 significant reduction in the action potential firing rate in both WT and *Fmr1* KO neurons (Fig.
211 3B). Together, our results from MEA and whole-cell patch-clamp recordings indicate that
212 activation of mGluR7 causes a decrease in neuronal network activity and excitability to a similar
213 degree in both WT and *Fmr1* KO cultures.

214 FXS patients and animal models all exhibit elevated circuit excitability with seizures as a
215 common comorbidity. The audiogenic seizure (AGS) test is commonly used to measure circuit
216 hyperexcitability in *Fmr1* KO mice (Ronesi *et al*, 2012), and we aimed to determine whether
217 activation of mGluR7 can reduce the susceptibility to AGS in *Fmr1* KO mice. We
218 intraperitoneally injected three-week-old *Fmr1* KO mice with saline or AMN082 (1 mg/kg). WT
219 mice were excluded from this experiment because they typically do not show audiogenic
220 seizures (Guo *et al*, 2016). Thirty minutes after the injection, the mice were presented with 110
221 dB via a personal alarm for 2 min while seizure behavior was scored (Fig. 3C top). As shown
222 (Fig. 3C bottom), treatment with AMN082 led to significant reduction in the susceptibility to
223 AGS in *Fmr1* KO mice. These results suggest that activation of mGluR7 can alleviate
224 pathological hyperexcitability in *Fmr1* KO mice.

225

226 **Activation of mGluR7 reduces autism-like behavior in *Fmr1* KO mice.**

227 Neural circuit hyperexcitability has been linked to other behavioral abnormalities in
228 *Fmr1* KO mice, such as repetitive behaviors (Hussein *et al*, 2023). Because activation of
229 mGluR7 can lead to a reduction in neuronal hyperexcitability in *Fmr1* KO neurons, we used the
230 marble burying test to assess the effect of mGluR7 on repetitive behavior in *Fmr1* KO mice. As

231 shown in Fig. 4A, saline-injected *Fmr1* KO mice buried significantly more marbles than saline-
232 injected WT mice, suggesting an elevation in repetitive behavior in *Fmr1* KO mice. Importantly,
233 injection of AMN082 (1 mg/kg) for 1 h corrects such a behavior in *Fmr1* KO mice but has no
234 effects in WT mice (Fig. 4A). This finding suggests that activation of mGluR7 leads to an
235 efficient reduction in repetitive behavior in *Fmr1* KO mice.

236 Because a marble burying test can be influenced by the animal's locomotion and anxiety
237 behavior, we used an open field test to assess these behaviors. Following treatment with saline or
238 AMN082, mice were allowed to explore an open field arena (67cm x 67cm) for 5 min. As shown
239 in Fig. 4B, based on measurements of the distance traveled, immobile time, and time in the
240 center zone, we did not observe any significant changes in WT or *Fmr1* KO mice treated with
241 either saline or AMN082. The saline injected *Fmr1* KO mice stayed slightly longer in the center
242 zone, but such an effect was not affected by AMN082 treatment. Together, we conclude that
243 AMN082 does not affect locomotion or anxiety behavior in WT or *Fmr1* KO mice.

244 Another commonly observed behavioral abnormality in FXS is impaired social
245 interaction (Gkogkas *et al*, 2014; Mineur *et al*, 2006; Fyke *et al*, 2018). We used a three-chamber
246 social interaction test to examine whether mGluR7 activation has an impact on social interaction.
247 The test was divided into two sessions. In the first session, the mouse was allowed to freely
248 explore and habituate in the arena. The second session was designed to test the sociability of the
249 test mouse with a stranger mouse (Fig. 4C). Sociability was measured by calculating the time the
250 test mouse spent interacting with the stranger mouse as opposed to the empty cage. Interestingly,
251 both WT and *Fmr1* KO mice showed similar sociability with the stranger mouse, and AMN082
252 did not produce significant effects. It is worth noting that studies in the field have reported
253 inconsistent observation regarding social interaction, locomotion, or anxiety in *Fmr1* KO mice

254 (Saré *et al*, 2016; Eadie *et al*, 2009). These discrepancies are likely caused by different genetic
255 background of the mice and different testing environment employed in each study. In conclusion,
256 our data suggests that activation of mGluR7 alleviates repetitive behavior without affecting
257 locomotion, anxiety, or sociability in *Fmr1* KO mice.

258

259 **Activation of mGluR7 improves learning and memory in *Fmr1* KO mice.**

260 Because FXS is associated with intellectual disability, we next investigated the effects of
261 mGluR7 activation on learning and memory in *Fmr1* KO mice. We first employed a novel object
262 recognition test to test object recognition memory. WT and *Fmr1* KO mice injected with saline
263 or AMN082 (1 mg/kg) were allowed to explore two identical objects during the first session,
264 followed by a second session where one of the two original objects was replaced with a novel
265 object. The behavior was videotaped and analyzed by Animal Tracker software (Gulyás *et al*,
266 2016), and the preference for novel objects was calculated (Fig. 5A, top). In comparison to WT
267 mice, *Fmr1* KO mice exhibited a reduction in recognition memory, demonstrated by a significant
268 reduction in preference index. Injection of AMN082 for 1 h corrected this phenotype in *Fmr1*
269 KO mice without significant effects in WT mice (Fig. 5A, bottom).

270 To further evaluate learning and memory, we applied a contextual fear conditioning test
271 to evaluate associative learning and memory, which has been shown to be impaired in *Fmr1* KO
272 mice (Ding *et al*, 2014). WT and *Fmr1* KO mice were injected with saline or AMN082 (1 mg/kg)
273 for 1 h and subjected to the test as shown in the schematic paradigm (Fig. 5B, top). Each test
274 session was videotaped, and the duration of freezing behavior was calculated as described earlier
275 (Lee *et al*, 2021). Saline-treated *Fmr1* KO mice exhibited significantly reduced freezing behavior

276 when compared with respective WT control mice. Notably, AMN082-treated *Fmr1* KO mice
277 showed a significant increase in freezing behavior, while AMN082 did not induce significant
278 effects in WT mice (Fig. 5B, bottom).

279 Because *Fmr1* KO mice have been shown to exhibit impaired spatial learning and
280 memory (Baker *et al*, 2010) we aimed to evaluate the effects of AMN082 on spatial learning and
281 memory using the Barnes maze test. During the test, the mouse was trained to locate the escape
282 box placed under one of the holes to escape from the high-intensity light. Three trials (5 min
283 each) were conducted each day for four days, and the average escape latency (time taken to
284 locate and enter the escape box) and the number of errors made before locating the escape box
285 were calculated. We did not observe any significant difference between WT and *Fmr1* KO mice
286 in escaping behavior across all four days, and AMN082 treatment did not produce any further
287 effects (Fig. 5C, top). On day 5, the mice were subject to a probe trial to assess spatial memory
288 formation where the escape box was removed, and the duration of time spent in the target
289 quadrant was measured. No significant difference was observed between WT and *Fmr1* KO mice,
290 and AMN082 did not produce any effects in either genotype (Fig. 5C, bottom). These results
291 suggest no spatial memory defects in this cohort of *Fmr1* KO mice, which was similarly seen by
292 other studies (Van Dam *et al*, 2000; Leach *et al*, 2016), and AMN082 did not lead to
293 improvements in this behavior. Altogether, these data suggest that activation of mGluR7
294 produced some improvement in learning and memory based on our data from novel object
295 recognition and contextual fear conditioning tests.

296

297

298

299

300 **DISCUSSION**

301 In this study, we found that activation of mGluR7 leads to a reduction in susceptibility to
302 AGS, reduction in repetitive behavior, and improvement in learning and memory in *Fmr1* KO
303 mice (Fig. 5D). Molecularly, we revealed repression of protein synthesis in an *Fmr1*-dependent
304 manner as a novel functional outcome of mGluR7 activation. This repression appears to take
305 place via inhibition of ERK1/2 and eIF4E phosphorylation, which is a common signaling
306 pathway involved in *de novo* protein synthesis (Waskiewicz *et al*, 1997; Pyronnet *et al*, 1999;
307 Joshi *et al*, 1995). Because activation of mGluR7 is known to inhibit adenylyl cyclase, it is
308 likely that reversed protein synthesis and behavior in *Fmr1* KO mice upon treatment of AMN082
309 are accompanied by reduction in cytosolic cAMP levels. This is consistent with the study by
310 Sethna *et al* (Sethna *et al*, 2017) showing increased cAMP in *Fmr1* KO mouse model due to
311 increased translation of type 1 adenylyl cyclase (*Adcy1*) mRNA, and its suppression improved
312 behavioral abnormalities in *Fmr1* KO mouse model. However, other recent studies have shown
313 lower cAMP levels in the human FXS cells as well as the mouse models of FXS (Berry-Kravis *et*
314 *al*, 1995; Kelley *et al*, 2007; Berry-Kravis & Sklena, 1993). It is also reported that increasing
315 cAMP levels using inhibitor of phosphodiesterase 4 (PDE4) significantly alleviated symptoms of
316 FXS (Gurney *et al*, 2017; Berry-Kravis *et al*, 2021; Rosenheck *et al*, 2021). These contradicting
317 studies suggest the complexity of molecular mechanism underlying behavioral abnormalities in
318 *Fmr1* KO animal models. They also support the need for a future direction to cross-examine age-,
319 brain region-, and cell type-specific effects observed in different studies.

320 Because activation of other glutamate receptors, such as N-methyl-D-aspartate (NMDA)
321 receptors, mGluR1, and mGluR5, is known to promote protein synthesis, our findings suggest
322 that mGluR7 activation potentially acts as a counterbalance to prevent overproduction of new
323 proteins upon activity-associated stimulation. To test this possibility in the future, we may need
324 to understand how different glutamate receptors regulate protein synthesis in distinct directions.
325 Does activity-dependent translational control occur via a biased manner where only certain types
326 of glutamate receptors are activated to achieve either elevation or reduction of protein synthesis?
327 Or does glutamate activate all possible glutamate receptors, but the effect on protein synthesis
328 depends on the availability of downstream signaling molecules that relay the information? Both
329 scenarios may be true and could potentially happen simultaneously, and we propose to test them
330 in a future study.

331 Our data indicate that activation of mGluR7 can repress protein synthesis in both WT and
332 *Fmr1* KO neurons, suggesting that the effects are *Fmr1*-independent. This prediction is expected
333 because no previous studies showing a dysregulation of mGluR7 in FXS patients or animal
334 models have been reported, although our results show a slightly altered surface expression
335 pattern of mGluR7a and mGluR7b in *Fmr1* KO mice. We therefore conclude that while *Grm7* is
336 not a disease-causing gene, activation of mGluR7 is useful for correcting or alleviating the
337 pathological defects in FXS. As we showed in this study, hyperexcitability, repetitive behavior,
338 and memory deficits in *Fmr1* KO mice were found to be significantly improved following
339 activation of mGluR7. Given the many functions of FMRP and the extensive binding affinity
340 toward numerous mRNAs by FMRP, the pathophysiology of FXS is extremely complex. We
341 tested several known defects in *Fmr1* KO mice, but it remains to be determined whether and how
342 mGluR7 activation can correct other reported phenotypes in FXS or its animal models. For

343 example, local protein synthesis in axons or dendrites especially for synaptic proteins is known
344 to be impaired in *Fmr1* KO mice (Daroles *et al*, 2016; Monday *et al*, 2022). It would be of
345 particular interest to determine whether activation of mGluR7 can correct local protein synthesis
346 in *Fmr1* KO neurons. Another example would be to study whether and how AMN082 can rescue
347 the excessive dendritic spines in *Fmr1* KO neurons. Furthermore, since mGluR7 is expressed in
348 both pre- and post-synaptic compartments (Palazzo *et al*, 2016), it will be important to study if
349 the suppression of protein synthesis upon activation of mGluR7 is mediated via pre- and/or post-
350 synaptic terminals. In addition, *Fmr1* KO mice exhibit multiple translation-related defects in
351 neural plasticity, including long-term potentiation (Tian *et al*, 2017), long-term depression (Niere
352 *et al*, 2012), and homeostatic plasticity (Lee *et al*, 2018; Soden & Chen, 2010). Given that
353 mGluR7 activation can repress protein synthesis in *Fmr1* KO neurons, we expect that
354 pharmacological activation of mGluR7 using AMN082 may improve, at least partially, one or
355 more of these plasticity mechanisms. All such mechanisms would require substantial future
356 efforts to validate. One major challenge remains unmet when targeting mGluR7 *in vivo* is the
357 availability of a stable agonist. At present AMN082 is a highly potent, blood-brain-barrier
358 permeable and commercially available mGluR7 agonist. However, its rapid breakdown in liver
359 cells reduces its bioavailability (Sukoff Rizzo *et al*, 2011). On the other hand, the metabolites
360 produced from breakdown of AMN082 are shown to have an affinity for serotonin transporter
361 SERT (Sukoff Rizzo *et al*, 2011). This issue limits chronic use of AMN082 *in vivo* and prompts
362 another future direction to synthesize a rather more stable alternative of AMN082 that could
363 improve the study of physiological functions of mGluR7 activation *in vivo*.

364 FXS is the most common cause of inherited autism and mGluR7 is encoded by an
365 autism-linked gene. The rescue effect upon mGluR7 activation in *Fmr1* KO mice suggests the

366 possibility that AMN082 may exert beneficial effects toward other ASDs, particularly those with
367 known defects in protein synthesis. For example, mutations or haploinsufficiency of phosphatase
368 and tensin homolog (*PTEN*) results in autism (Butler *et al*, 2005) with elevated protein synthesis
369 being one of the most common defects observed in disease animal models⁵⁹. *PTEN*-associated
370 ASD also shares many similar phenotypes with FXS, including sensory hypersensitivity and
371 seizures (Smith *et al*, 2016). Another example is tuberous sclerosis complex, which shares
372 similar defects in protein synthesis as *PTEN*-associated ASD in addition to exhibiting seizure
373 phenotypes (Di Nardo *et al*, 2009). It would be of particular interest to examine whether
374 activation of mGluR7 can have a broader impact on other ASDs to reduce the hyperexcitability
375 phenotypes and perhaps also improve cognition. In summary, targeting mGluR7 has the potential
376 to open new avenues for the study of activity-dependent neural plasticity and neurodevelopment
377 with possibilities to introduce new approaches to produce improvements in the quality of life of
378 individuals affected by ASD. More research is needed and expected to broaden our
379 understanding of mGluR7, which is strongly associated with autism but remains poorly
380 understood.

381

382

383 **MATERIALS AND METHODS**

384

385 **Animals**

386 All experiments using animals followed the guidelines of Animal Care and Use provided by the
387 Illinois Institutional Animal Care and Use Committee (IACUC) and the guidelines of the

388 Euthanasia of Animals provided by the American Veterinary Medical Association (AVMA) to
389 minimize animal suffering and the number of animals used. This study was performed under an
390 approved IACUC animal protocol of University of Illinois at Urbana-Champaign (#20049 and
391 #23016 to N.-P. Tsai.). We obtained WT (stock No. 00664) and *Fmr1* KO mice (stock No.
392 003025) from Jackson laboratory and *Grm7* KO mice from MMRRC (B6.129P2-
393 *Grm7tm1Dgen/Mmnc*, stock No. 011626-UNC). Because of the higher prevalence of FXS in
394 males, we only employed male mice in our study. Mice were housed in individually ventilated
395 cages in 12 hrs light/dark cycle with *ad libitum* access to pelleted food and water. Although
396 experiments were not performed using littermate mice, WT and *Fmr1* KO littermates were used
397 to generate WT and *Fmr1* KO breeding cages. *Grm7* KO mice were identified by PCR with
398 genomic DNA prepared from toe clips. For genotyping *Grm7* deleting allele, we used primers
399 that detect *LacZ* allele to reflect the transgene: 5'- CGATCGTAATCACCCGAGTGT -3', and
400 5'- CCGTGGCCTGACTCATTCC -3'. The primers used to differentiate *wild-type* allele are 5'-
401 GCGGATCCTGGACACTTGTT -3', and 5'- GCGCCTGGACGAAAGTGA. For genotyping
402 *Fmr1* deleting allele, a set of three primers were used: 5'- CACGAGACTAGTGAGACGTG -3'
403 (*Fmr1* KO), 5'- CACGAGACTAGTGAGACGTG -3' (*wild-type*), and 5'-
404 CTTCTGGCACCTCCAGCTT -3' (common reverse primer).

405

406 **Primary neuronal culture**

407 The primary cortical neuronal culture was performed as previously described using mice at post-
408 natal day 0-1 (Tsai *et al*, 2012). Cortices were dissected and incubated with trypsin for 8-10 mins
409 at 37°C. Next, trypsin was neutralized by the addition of fetal bovine serum (FBS) supplemented
410 HBSS and washed twice with pre-warm HBSS. Cortices were then briefly homogenized in

411 complete DMEM and plated on poly-D-lysine (0.05 mg/ml) coated 6-well plates. After 3-5 hrs,
412 the medium was replaced with Neurobasal A medium (10888022, ThermoFisher Scientific)
413 supplemented with 2 mM Glutamax (35050061, Invitrogen), B27 supplement (17504001,
414 Invitrogen) and 1 μ M Ara-C ((β -D-Arabinofuranosyl) cytosine) (C1768, Sigma-Aldrich).
415 Cultures were maintained at 37°C with 5% CO₂. Half of the medium was changed on days-in-
416 vitro (DIV) 2 and thereafter every 3-4 days. Experiments were performed when cultures were at
417 DIV 14-16.

418

419 **Reagents**

420 Dimethyl sulfoxide was from Thermo Fisher Scientific (#BP231). Antibodies for western
421 blotting were purchased from Sigma: rabbit anti-mGluR7a (#07-239, 1:2000 dilution) and mouse
422 anti-puromycin (#MABE343, 1:1000 dilution); from Synaptic Systems: rabbit anti-mGluR7b
423 (#191 203, 1:2000 dilution); from Proteintech: anti-GAPDH (#60004-1, 1:2500); from Thermo
424 Fisher Scientific: rabbit anti-phospho-eIF2 α (#MA5-15133, 1:1000 dilution); from Bioss: rabbit
425 anti-PCDH7 (#bs-11085R, 1:1000 dilution); from Abcam: anti-phospho-eIF4E (#2069, 1:1000
426 dilution); from Cell Signaling Technology: rabbit anti-FMRP (#7104, 1:2500 dilution); rabbit
427 anti-N-cadherin (#13116, 1:2500 dilution); rabbit anti-ERK1/2 (#4695, 1:5000 dilution); rabbit
428 anti-phospho-ERK1/2 (#4370, 1:5000 dilution); rabbit anti-mTOR (#2972, 1:2500 dilution),
429 rabbit anti-phospho-mTOR (#2971, 1:2500 dilution); rabbit anti-eIF4E (#2067, 1:2500 dilution);
430 rabbit anti-eIF2 α (#5324, 1:2500 dilution); rabbit anti-eIF4G (#2498, 1:2500 dilution).
431 Secondary antibodies were from Cell Signaling Technology: anti-mouse HRP (#7076, 1:2500
432 dilution) and from Jackson ImmunoResearch: anti-rabbit HRP (#711-035-152, 1:2500 dilution).

433

434 **Western blotting**

435 Tissue or cell cultures were lysed in ice-cold lysis buffer (137mM NaCl, 20 mM Tris-HCL,
436 2mM EDTA and 1% Triton X-100, pH 8.0) supplemented with protease inhibitors (A32963,
437 ThermoFisher Scientific) and phosphatase inhibitors (P2850; Sigma-Aldrich). Lysates were
438 briefly sonicated and centrifuged. Supernatants were collected and protein concentration was
439 measured using Bradford's method. SDS buffer (40% glycerol; 240 mM Tris-HCl, pH 6.8; 8%
440 sodium dodecyl sulfate; 0.04% bromophenol blue; and 5% β -mercaptoethanol) was added to the
441 lysates and heated at 95°C for 10 mins. Samples were then separated on SDS-PAGE gel and
442 transferred onto a PVDF membrane (sc-3723, Santa Cruz Biotechnology). Membranes were
443 blocked with 1% bovine serum albumin (BSA, BP9706100, ThermoFisher Scientific) in Tris-
444 buffered saline Tween-20 buffer (TBST; [20 mM Tris, pH 7.5; 150 mM NaCl; 0.1% Tween-20])
445 for 30 mins. Subsequently, membranes were incubated with primary antibodies overnight at 4°C.
446 Next, the membranes were washed 3 times in TBST and incubated with HRP-conjugated
447 secondary antibody in 5% non-fat skimmed milk in TBST for an hour at 25°C. Membranes were
448 washed with TBST for 3 times and developed by using an enhanced chemiluminescence reagent
449 and detected by an iBright imaging system (ThermoFisher Scientific, Waltham, MA). Band of
450 the protein of interest were analyzed by ImageJ software (National Institute of Health).

451

452 **Surface protein biotinylation**

453 For surface biotinylation, primary cortical neurons were plated at a density of 5×10^6 per well in
454 6-well plates as described previously (Nair *et al*, 2021). Cultures at DIV 14-16 were incubated

455 on ice for 10 mins followed by washing twice with DPBS (Dulbecco's phosphate-buffered saline,
456 ThermoFisher Scientific 14200-059). Cultures were then biotin-labelled by incubating with 0.3
457 mg/ml Sulfo-NHS-SS-biotin (21331, ThermoFisher Scientific) solution for 10 mins. Unbound
458 biotin was scavenged by adding 100 mM NH₄Cl followed by three washes with DPBS. Biotin-
459 labelled cultures were then lysed in ice-cold lysis buffer and sonicated briefly. Lysates were
460 centrifuged and supernatants were incubated with Streptavidin-Agarose beads (S1638, Merck)
461 for an hour at 4°C. After incubation, the lysates were removed by centrifugation and pelleted
462 Streptavidin-Agarose beads were incubated with 4x sample buffer at 95 °C for 10 minutes to
463 elute biotin-labelled surface proteins from beads. Eluted biotin-labelled surface protein was
464 processed for western blotting as described above.

465

466 **m7GTP pull-down assay**

467 m7GTP pull-down assay was performed in WT and *Fmr1* KO primary neuron cultures. The
468 assay was performed as previously described (Santini *et al*, 2017). In brief, following treatment
469 of DMSO or AMN082, neurons were harvested and sonicated in ice cold lysis buffer (137mM
470 NaCl, 20 mM Tris-HCL, 2mM EDTA and 1% Triton X-100, pH 8.0) supplemented with
471 protease inhibitors (A32963, ThermoFisher Scientific) and phosphatase inhibitors (P2850;
472 Sigma-Aldrich). Two hundred µg protein from each treatment condition was incubated with 20
473 µl m7GTP beads (m7GTP-001A, Creative BioMart) on a rotating mixer for 2 hours. Following
474 incubation, beads were pelleted by centrifugation at 6000 rpm for 1 min. Beads were then
475 washed three times using cold lysis buffer. The protein complexes bound by the m7GTP beads
476 were eluted in 4X SDS buffer and subjected to western blotting.

477

478 **Immunohistochemistry and imaging**

479 Mice were anaesthetized using isoflurane inhalation and transcardially perfused with PBS
480 containing 10 units /ml heparin sodium (411210010, ThermoFisher Scientific) followed by 4%
481 paraformaldehyde (PFA). The brains harvested were stored in 4% PFA overnight and then
482 transferred to 10, 20 and 30% sucrose solution every 24 hrs at 4°C. Brains were then
483 cryosectioned in Leica 3050S cryotome and 15 µm sections were obtained. For immunostaining,
484 sections were placed on gelatin-coated slides and incubated in antigen unmasking solution (H-
485 3300, Vector Labs) at 70°C for 40 mins in a water bath. Sections were washed 3 times with PBS
486 for 5 mins each and permeabilized with 0.3% triton-x 100 for 10 mins and then blocked with
487 blocking buffer (1% bovine serum albumin, 3% normal goat serum and 0.3% triton-x 100) for 1
488 hr at 25°C. Sections were then probed with primary antibody prepared in blocking buffer and
489 incubated overnight at 4°C with anti-mGluR7a antibody (ab302530, Abcam, 1:250 dilution).
490 Sections were washed with PBS and probed with Alexa488-conjugated goat anti-rabbit
491 secondary antibody (BA-1000-1.5, Vector Labs) prepared in PBS at 1:1000 dilution and
492 incubated for 2 hrs at 25°C. Sections were washed with PBS and mounted using a mounting
493 medium with DAPI (P36931, ThermoFisher Scientific). Imaging was performed in Zeiss LSM
494 700 Confocal microscope using 405 and 488 nm lasers. Images were acquired in z-stacks with
495 20X objective at 0.5X digital zoom and were processed using ImageJ software (National Institute
496 of Health).

497

498 **MEA recording**

499 Multielectrode array (MEA) recordings were performed using Maestro Edge (Axion Biosystems)
500 with Cytoview MEA6 plates (6-well plates). Field potentials were recorded at each electrode
501 relative to the ground electrode with a sampling frequency of 12.5 kHz. Followed by 30 mins
502 baseline recording (before), neurons were treated with indicated drugs for 2 hrs and recorded for
503 another 30 minutes. To avoid the effect of change in physical movement on network activity,
504 only the last 15 minutes of the recordings were used for data analysis. Axis Navigator version 3.3
505 software (Axion Biosystems) was used for spike extraction from raw electrical signals. After
506 filtering the spike detector setting for each electrode was independently set at the threshold of ± 6
507 standard deviation. Therefore, activity above the threshold was counted as a spike and included
508 in data for analysis as previously described (Jewett *et al*, 2016). The total number of spikes was
509 normalized to the number of electrodes in each well. The average number of spikes was
510 calculated and expressed as fold changes with respect to the control. For detection of burst, a
511 minimum of 5 spikes with a maximum 100 ms spike interval was set for individual electrodes as
512 described earlier (Jewett *et al*, 2016). Analysis of burst duration and burst frequency was
513 performed using Axis Navigator version 3.3 software.

514

515 **Whole-cell patch clamp recordings**

516 Whole-cell patch clamp recordings of action potential (AP) firing were carried out at 23-25°C in
517 a submersion chamber continuously perfused with ACSF containing (in mM): 119 NaCl, 2.5
518 KCl, 4 CaCl₂, 4 MgCl₂, 1 NaH₂PO₄, 26 NaHCO₃ and 11 D-Glucose, saturated with 95% O₂/5%
519 CO₂ (pH 7.4, 310 mOsm), and were performed in the presence of fast synaptic transmission
520 blockers: CNQX (20 μ M); DL-APV (200 μ M); and PTX (100 μ M). Recording pipettes had a
521 resistance of 4–6 M Ω when filled with an internal solution containing (in mM): 130 K-gluconate,

522 6 KCl, 3 NaCl, 10 HEPES, 0.2 EGTA, 4 Mg-ATP, 0.4 Na-GTP, 14 Tris-phosphocreatine (pH
523 7.25, 285 mOsm). Neurons were held at -60 mV. Action potential firing rates were measured
524 upon delivering constant current pulses of 500 ms in the range 0–200 pA, and the number of
525 action potentials was averaged from 3 to 5 individual sweeps for current intensity. Neurons were
526 omitted if the resting membrane potential was ≥ 50 mV or if no action potentials were discharged.
527 No series resistance compensation was used. The data were recorded using a Multiclamp 700B
528 amplifier, Digidata 1550B, and the pClamp 10.6 (Molecular Devices). Recordings were filtered
529 at 2 kHz and digitized at 10 kHz. Data analyses were performed using Clampfit 10.6 (Molecular
530 Devices).

531

532 ***In vivo* puromycin labeling**

533 Six-to-eight weeks old WT, *Fmr1* KO and *mGluR7*KO mice were intraperitoneally injected with
534 saline or AMN082 (1 mg/kg) and puromycin (200 mg/kg). One hour after the injections, mice
535 were anaesthetized using isoflurane inhalation and hippocampi were dissected out and flash
536 frozen in liquid N₂. Hippocampi were then lysed in ice cold lysis buffer by sonication. Lysates
537 were incubated with 4X SDS buffer at 95 °C for 10 minutes and subjected to western blotting.

538

539 **Audiogenic seizure assay**

540 *Fmr1* KO mice at post-natal day 20-22 were kept in a standard housing cage with minimum
541 external noise to avoid auditory desensitization. Animals were intraperitoneally injected with
542 saline or AMN082 (1 mg/kg). After 30 mins, the mice were habituated in the transparent plastic
543 box (28x17.5x12 cm) for 2 mins before the onset of an auditory stimulus of 110 dB SPL

544 (Personal alarm, Radioshack model 49–1010) for 2 minutes. The mice were videotaped during
545 this time and scored for behavioral phenotype: 0=no response, 1=wild running, 2=tonic-clonic
546 seizures, 3=status epilepticus and 4=death as described previously (Ronesi et al, 2012).

547

548 **Behavioral tests**

549 All the behavioral tests were conducted on WT and *Fmr1* KO mice at 6-8 weeks of age weighing
550 24-27 g unless otherwise specified. Mice were brought to the behavior testing room 30 minutes
551 before the test and housed in their home cages. The room was dimly lit at 50 lux and low
552 background noise (approx. 65 db). Behavioral apparatuses were thoroughly cleaned before and
553 after every test session with 70% ethanol to avoid olfactory bias. Detailed procedures are
554 provided below.

555

556 **Marble burying test**

557 In a polycarbonate cage (26 x 48 x 20 cm) a total of 20 marbles were placed on the surface of
558 bedding which was approximately 5 cm deep. Marbles were arranged in a 5x4 array. Mouse was
559 introduced into the cage and allowed to remain inside for 30 minutes. Afterwards, the mouse was
560 taken out and a photograph of the cage floor was taken, and the total number of buried marbles
561 was counted. A marble was classified as "buried" if two-thirds or more of it was concealed
562 beneath the bedding. To carry out the next set of experiments, a clean cage filled with new
563 bedding and marbles was used, following the same procedure as above.

564

565 **Open field test**

566 The open field test was carried out to evaluate the locomotion and anxiety behavior of mice. The
567 mouse was placed in the centre of a plexiglass box (67 x 67 x 31 cm) and allowed to freely
568 explore the arena for 5 minutes. The movement of the mouse was recorded with an overhead
569 camera and the video was analyzed using the AnimalTracker plugin in ImageJ (National Institute
570 of Health). The open-field arena was virtually divided into central and outer zones. The
571 movement trajectory, velocity, immobile time, and total distance travelled by the test animal
572 were calculated.

573

574 **Social interaction test**

575 The social interaction test was conducted in a plexiglass chamber measuring 20 x 40 x 25 cm and
576 was divided into 3 parts by transparent walls with small openings to allow free movement of test
577 animals between all three compartments. The test consisted of 3 sessions: habituation,
578 sociability, and social novelty sessions. Each session lasted for 10 mins and was video recorded
579 using an overhead camera. During the habituation session, the mouse was introduced to the
580 middle chamber and allowed to explore all three chambers. For the sociability session, a stranger
581 mouse of the same age and sex was placed in a wired cylinder and placed in the left chamber
582 while an empty wired cylinder was placed in the right chamber. The test mouse was then
583 reintroduced into the middle chamber and allowed to explore the left and the right chamber. For
584 the social novelty session, the second strange mouse was kept in the wired cylinder and placed in
585 the right chamber. The test mouse was then reintroduced into the middle chamber and allowed to
586 explore both stranger mice. The video from the second and third sessions was analyzed to

587 calculate sociability and social novelty. The time spent by the test mouse to interact with the
588 first stranger mouse over an empty cage was represented as sociability. The time spent
589 interacting with the second stranger mouse was represented as a social novelty.

590

591 **Novel Object Recognition test**

592 To test the object recognition memory, novel object recognition test was performed as previously
593 described (Lee *et al*, 2021). On day-1 (trial day), the mouse was placed in the empty testing
594 chamber (25 x 25 cm) and allowed to habituate for 10 min, during which the mouse was allowed
595 to freely explore two identical objects in the box before returning to the home cage. On day 2
596 (testing day), one of the two identical objects was replaced with a novel object and the mouse
597 was allowed to explore them for 10 minutes. The preference for exploring the novel object was
598 calculated by dividing the time elapsed by the mouse exploring the novel object (T_{novel}) by the
599 time elapsed for exploring both familiar and novel objects ($T_{\text{novel}}+T_{\text{familiar}}$) and expressed as the
600 preference index i.e. ($T_{\text{novel}}/(T_{\text{novel}}+T_{\text{familiar}}) \times 100$).

601

602 **Contextual fear conditioning**

603 The test mice were divided into two groups: the fear group (receiving foot shock) and the control
604 group (not receiving foot shock). The experiment was carried out in two days. On the first day
605 (training phase), the mice were placed inside the fear conditioning chamber (32 x 28 x 30 cm)
606 with a metal grid floor for 3 minutes. The fear group received two foot shocks of 0.5 mA for 2
607 seconds at 120 sec and 150 sec. The control group was also placed in the box for 3 minutes but
608 did not receive any foot shock. After 3 minutes the test mice were returned to their home cage.

609 On the second day, both the control group and the fear group were placed in the fear
610 conditioning chamber for 3 mins. At this time no foot shock was delivered to either group. Each
611 session was video-recorded and analyzed for freezing behavior. Freezing time was calculated
612 and represented as the freezing percentage.

613

614 **Barnes maze test**

615 The test lasted for six days and was divided into 3 phases: adaptation session on day 0, spatial
616 acquisition trial from day 1 to 4 and probe trial on day 5. The test mouse was placed in the center
617 of a gray circular platform having 20 evenly spaced holes on its perimeter. A bright light of
618 1,200 lux was used as a negative reinforcement stimulus that motivated mice to locate the escape
619 box which was placed underneath one of the 20 holes. During the adaptation session, each test
620 mouse was placed on the platform and allowed to explore the arena for 5 minutes to locate the
621 hole with the escape box. If the mouse failed to locate the escape box it was gently guided to the
622 escape box. Next, for the spatial-acquisition session, the mice were placed on the platform for 5
623 minutes and allowed to find the escape box. The escape box was immediately closed after the
624 mouse entered the box and allowed the mice to stay in the box for two minutes. This helps them
625 to associate the escape box as a safe place. Three consecutive trials were done each day for 4
626 days. The probe trial was done on day 5 where the escape box under the target hole was removed
627 and the test animal was allowed to explore the arena for 2 mins under bright light as above. All
628 the trials were video recorded and analyzed using ImageJ software. The latency to find the
629 escape box and the number of errors made while locating the escape box were calculated for all
630 the special-acquisition trials. For assessment of the probe trial, the circular platform was divided
631 into 4 quadrants and time spent by the mice in the target quadrant (quadrant with the initial target

632 hole) was calculated and represented as target quadrant occupancy.

633

634 **Experimental Design and Statistical Analysis**

635 Student's *t*-test was used when two conditions or groups were compared. Two-way ANOVA
636 with *post hoc* Tukey or Šidák's HSD test was used when making multiple comparisons. Two-
637 tailed Mann-Whitney test was performed as non-parametric test to compare two groups when the
638 criteria for Student's *t*-test was not met. Due to the design of our research, no blinding was
639 performed. Specific sample numbers, including the numbers of cells or repeats, are indicated in
640 the figure legends. The sample size was estimated by G*Power 3.1. No samples or animals were
641 excluded from our analyses. The data presented in this study have been tested for normality
642 using the Kolmogorov-Smirnov test. Data analyses were performed using GraphPad Prism
643 software. Differences are considered significant when $p < 0.05$.

644

645 **DATA AVAILABILITY**

646 This study includes no data deposited in external repositories.

647

648

649 **ACKNOWLEDGEMENTS**

650 This work is supported by National Institute of Health R01MH124827 and
651 R21NS130751 to N-P.T as well as a FRAXA Research Foundation Postdoctoral Fellowship to
652 V.K.

653

654

655 **DISCLOSURE AND COMPETING INTERESTS STATEMENT**

656 The authors declare no competing interests.

657

658

659 **THIS PAPER EXPLAINED**

660 Problem:

661 Fragile X syndrome (FXS) is caused by the lack of fragile X messenger
662 ribonucleoprotein (FMRP) that is encoded by the *Fmr1* gene. FXS patients and the mouse model
663 of FXS, the *Fmr1* KO mice, all exhibit excessive protein synthesis, which is central to most
664 disease-specific molecular and behavioral defects in FXS. However, there remains no effective
665 treatment for FXS.

666 Results:

667 Here, we showed that a positive allosteric modulator for mGluR7, AMN082, effectively
668 represses protein synthesis by reducing phosphorylation of ERK1/2 and eIF4E. This translational
669 suppressive effect appears to be *Fmr1*-independent. We further showed that treatments of
670 AMN082 reduce neuronal excitability and susceptibility to audiogenic seizures in *Fmr1* KO
671 mice. Lastly, treatments of AMN082 alleviate repetitive behavior and improve learning and
672 memory in *Fmr1* KO mice.

673 Impact:

674 Our results uncover the novel roles of mGluR7 and AMN082 in translational control and
675 suggest activation of mGluR7 as a potential therapeutic approach for treating FXS. Given that

676 FXS presents with symptoms that are common to many other neurological and psychiatric
677 disorders, our findings also introduce mGluR7 as a novel therapeutic target for other diseases
678 that are associated with uncontrolled protein synthesis.

679

680 **FOR MORE INFORMATION:**

681 More information about FXS can be found at Fragile X Research Foundation website
682 (<https://www.fraxa.org/>).

683

684

685

686

687 **REFERENCES**

688 Baker KB, Wray SP, Ritter R, Mason S, Lanthorn TH & Savelieva K V. (2010) Male and female
689 Fmr1 knockout mice on C57 albino background exhibit spatial learning and memory
690 impairments. *Genes Brain Behav* 9

691 Berry-Kravis E, Hicar M & Ciurlionis R (1995) Reduced cyclic AMP production in fragile X
692 syndrome: Cytogenetic and molecular correlations. *Pediatr Res* 38

693 Berry-Kravis E, Des Portes V, Hagerman R, Jacquemont S, Charles P, Visootsak J, Brinkman M,
694 Rerat K, Koumaras B, Zhu L, *et al* (2016) Mavoglurant in fragile X syndrome: Results of
695 two randomized, double-blind, placebo-controlled trials. *Sci Transl Med* 8

696 Berry-Kravis E, Raspa M, Loggin-Hester L, Bishop E, Holiday D & Bailey DB (2010) Seizures
697 in fragile X syndrome: characteristics and comorbid diagnoses. *Am J Intellect Dev Disabil*
698 115: 461–472

699 Berry-Kravis E & Sklena P (1993) Demonstration of abnormal cyclic AMP production in
700 platelets from patients with fragile X syndrome. *Am J Med Genet* 45

701 Berry-Kravis EM, Harnett MD, Reines SA, Reese MA, Ethridge LE, Outterson AH, Michalak C,
702 Furman J & Gurney ME (2021) Inhibition of phosphodiesterase-4D in adults with fragile X
703 syndrome: a randomized, placebo-controlled, phase 2 clinical trial. *Nat Med* 27

704 Bhakar AL, Dölen G & Bear MF (2012) The pathophysiology of fragile X (and what it teaches
705 us about synapses). *Annu Rev Neurosci* 35 doi:10.1146/annurev-neuro-060909-153138
706 [PREPRINT]

707 Bolduc F V., Bell K, Cox H, Broadie KS & Tully T (2008) Excess protein synthesis in
708 *Drosophila* Fragile X mutants impairs long-term memory. *Nat Neurosci* 11

709 Bradley SR, Levey AI, Hersch SM & Conn PJ (1996) Immunocytochemical localization of
710 group III metabotropic glutamate receptors in the hippocampus with subtype-specific
711 antibodies. *Journal of Neuroscience* 16

712 Budimirovic DB & Kaufmann WE (2011) What can we learn about autism from studying fragile
713 X syndrome? *Dev Neurosci* 33 doi:10.1159/000330213 [PREPRINT]

714 Butler MG, Dazouki MJ, Zhou XP, Talebizadeh Z, Brown M, Takahashi TN, Miles JH, Wang
715 CH, Stratton R, Pilarski R, *et al* (2005) Subset of individuals with autism spectrum
716 disorders and extreme macrocephaly associated with germline PTEN tumour suppressor
717 gene mutations. *J Med Genet* 42

718 Dalezios Y, Luján R, Shigemoto R, Roberts JDB & Somogyi P (2002) Enrichment of mGluR7a
719 in the presynaptic active zones of GABAergic and non-GABAergic terminals on
720 interneurons in the rat somatosensory cortex. *Cerebral Cortex* 12

721 Van Dam D, D’Hooge R, Hauben E, Reyniers E, Gantois I, Bakker CE, Oostra BA, Kooy RF &
722 De Deyn PP (2000) Spatial learning, contextual fear conditioning and conditioned
723 emotional response in *Fmr1* knockout mice. *Behavioural Brain Research* 117

724 Daroles L, Gribaudo S, Doulazmi M, Scotto-Lomassese S, Dubacq C, Mandairon N, Greer CA,
725 Didier A, Trembleau A & Caillé I (2016) Fragile X Mental Retardation Protein and
726 Dendritic Local Translation of the Alpha Subunit of the Calcium/Calmodulin-Dependent
727 Kinase II Messenger RNA Are Required for the Structural Plasticity Underlying Olfactory
728 Learning. *Biol Psychiatry* 80

729 Dasgupta A, Lim YJ, Kumar K, Baby N, Pang KKL, Benoy A, Behnisch T & Sajikumar S (2020)
730 Group III metabotropic glutamate receptors gate long-term potentiation and synaptic
731 tagging/capture in rat hippocampal area CA2. *Elife* 9

732 Ding Q, Sethna F & Wang H (2014) Behavioral analysis of male and female *Fmr1* knockout
733 mice on C57BL/6 background. *Behavioural Brain Research* 271

734 Dölen G & Bear MF (2008) Role for metabotropic glutamate receptor 5 (mGluR5) in the
735 pathogenesis of fragile X syndrome. In *Journal of Physiology*

736 Dölen G, Osterweil E, Rao BSS, Smith GB, Auerbach BD, Chattarji S & Bear MF (2007)
737 Correction of Fragile X Syndrome in Mice. *Neuron* 56

738 Eadie BD, Zhang WN, Boehme F, Gil-Mohapel J, Kainer L, Simpson JM & Christie BR (2009)
739 Fmr1 knockout mice show reduced anxiety and alterations in neurogenesis that are specific
740 to the ventral dentate gyrus. *Neurobiol Dis* 36

741 Fisher NM, Seto M, Lindsley CW & Niswender CM (2018) Metabotropic glutamate receptor 7:
742 A new therapeutic target in neurodevelopmental disorders. *Front Mol Neurosci* 11
743 doi:10.3389/fnmol.2018.00387 [PREPRINT]

744 Fyke W, Corf KL, Ginger M, Frick A & Pietropaolo S (2018) BKca channels during early
745 developmental periods as therapeutic targets for fragile x syndrome. *Ann Neurol* 84

746 Gkogkas CG, Khoutorsky A, Cao R, Jafarnejad SM, Prager-Khoutorsky M, Giannakas N,
747 Kaminari A, Fragkouli A, Nader K, Price TJ, *et al* (2014) Pharmacogenetic Inhibition of
748 eIF4E-Dependent Mmp9 mRNA Translation Reverses Fragile X Syndrome-like Phenotypes.
749 *Cell Rep* 9

750 Gu Z, Liu W, Wei J & Yan Z (2012) Regulation of N-methyl-D-aspartic acid (NMDA) receptors
751 by metabotropic glutamate receptor 7. *Journal of Biological Chemistry* 287

752 Gulyás M, Bencsik N, Pusztai S, Liliom H & Schlett K (2016) AnimalTracker: An ImageJ-
753 Based Tracking API to Create a Customized Behaviour Analyser Program.
754 *Neuroinformatics* 14 doi:10.1007/s12021-016-9303-z [PREPRINT]

755 Guo W, Molinaro G, Collins KA, Hays SA, Paylor R, Worley PF, Szumlinski KK & Huber KM
756 (2016) Selective disruption of metabotropic glutamate receptor 5-homer interactions mimics
757 phenotypes of fragile X syndrome in mice. *Journal of Neuroscience* 36

758 Gurney ME, Cogram P, Deacon RM, Rex C & Tranfaglia M (2017) Multiple Behavior
759 Phenotypes of the Fragile-X Syndrome Mouse Model Respond to Chronic Inhibition of
760 Phosphodiesterase-4D (PDE4D). *Sci Rep* 7

761 Hagerman RJ, Berry-Kravis E, Hazlett HC, Bailey DB, Moine H, Kooy RF, Tassone F, Gantois I,
762 Sonenberg N, Mandel JL, *et al* (2017) Fragile X syndrome. *Nat Rev Dis Primers* 3

763 Hagerman RJ, Berry-Kravis E, Kaufmann WE, Ono MY, Tartaglia N, Lachiewicz A, Kronk R,
764 Delahunty C, Hessel D, Visootsak J, *et al* (2009) Advances in the treatment of fragile x
765 Syndrome. *Pediatrics* 123 doi:10.1542/peds.2008-0317 [PREPRINT]

766 Hagerman RJ & Hagerman PJ (2022) Fragile X Syndrome: Lessons Learned and What New
767 Treatment Avenues Are on the Horizon. *Annu Rev Pharmacol Toxicol* 62

768 Hölscher C, Schmid S, Pilz PKD, Sansig G, Van Der Putten H & Plappert CF (2005) Lack of the
769 metabotropic glutamate receptor subtype 7 selectively modulates Theta rhythm and working
770 memory. *Learning and Memory* 12

771 Hussein Y, Tripathi U, Choudhary A, Nayak R, Peles D, Rosh I, Rabinski T, Djamus J, Vatine
772 GD, Spiegel R, *et al* (2023) Early maturation and hyperexcitability is a shared phenotype of
773 cortical neurons derived from different ASD-associated mutations. *Transl Psychiatry* 13:
774 246

775 Jewett KA, Christian CA, Bacos JT, Lee KY, Zhu J & Tsai NP (2016) Feedback modulation of
776 neural network synchrony and seizure susceptibility by Mdm2-p53-Nedd4-2 signaling. *Mol*
777 *Brain* 9

778 Joshi B, Cai AL, Keiper BD, Minich WB, Mendez R, Beach CM, Stepinski J, Stolarski R,
779 Darzynkiewicz E & Rhoads RE (1995) Phosphorylation of eukaryotic protein synthesis
780 initiation factor 4E at Ser-209. *Journal of Biological Chemistry* 270

781 Kelley DJ, Davidson RJ, Elliott JL, Lahvis GP, Yin JCP & Bhattacharyya A (2007) The cyclic
782 AMP cascade is altered in the fragile X nervous system. *PLoS One* 2

783 Kim HW, Ha SH, Lee MN, Huston E, Kim D-H, Jang SK, Suh P-G, Houslay MD & Ryu SH
784 (2010) Cyclic AMP Controls mTOR through Regulation of the Dynamic Interaction
785 between Rheb and Phosphodiesterase 4D. *Mol Cell Biol* 30

786 Kinzie JM, Saugstad JA, Westbrook GL & Segerson TP (1995) Distribution of metabotropic
787 glutamate receptor 7 messenger RNA in the developing and adult rat brain. *Neuroscience* 69

788 Leach PT, Hayes J, Pride M, Silverman JL & Crawley JN (2016) Normal performance of Fmr1
789 mice on a touchscreen delayed nonmatching to position working memory task. *eNeuro* 3

790 Lee KY, Jewett KA, Chung HJ & Tsai NP (2018) Loss of fragile X protein FMRP impairs
791 homeostatic synaptic downscaling through tumor suppressor p53 and ubiquitin E3 ligase
792 Nedd4-2. *Hum Mol Genet* 27

793 Lee KY, Zhu J, Cutia CA, Christian-Hinman CA, Rhodes JS & Tsai NP (2021) Infantile spasms-
794 linked Nedd4-2 mediates hippocampal plasticity and learning via cofilin signaling. *EMBO*
795 *Rep* 22: e52645

796 Liu D, Li J, Lin H, Lorsung E, Le N, Singla R, Mishra A, Fukunaga R & Cao R (2022) Circadian
797 activities of the brain MNK-eIF4E signalling axis contribute to diurnal rhythms of some
798 cognitive functions. *European Journal of Neuroscience* 56

799 Liu DC, Lee KY, Lizarazo S, Cook JK & Tsai NP (2021) ER stress-induced modulation of
800 neural activity and seizure susceptibility is impaired in a fragile X syndrome mouse model.
801 *Neurobiol Dis* 158

802 Martín R, Torres M & Sánchez-Prieto J (2007) mGluR7 inhibits glutamate release through a
803 PKC-independent decrease in the activity of P/Q-type Ca²⁺ channels and by diminishing
804 cAMP in hippocampal nerve terminals. *European Journal of Neuroscience* 26

805 McCamphill PK, Stoppel LJ, Senter RK, Lewis MC, Heynen AJ, Stoppel DC, Sridhar V, Collins
806 KA, Shi X, Pan JQ, *et al* (2020) Selective inhibition of glycogen synthase kinase 3 α
807 corrects pathophysiology in a mouse model of fragile X syndrome. *Sci Transl Med* 12

808 Michalon A, Sidorov M, Ballard TM, Ozmen L, Spooren W, Wettstein JG, Jaeschke G, Bear MF
809 & Lindemann L (2012) Chronic Pharmacological mGlu5 Inhibition Corrects Fragile X in
810 Adult Mice. *Neuron* 74

811 Millán C, Luján R, Shigemoto R & Sánchez-Prieto J (2002) The inhibition of glutamate release
812 by metabotropic glutamate receptor 7 affects both $[Ca^{2+}]_c$ and cAMP. Evidence for a
813 strong reduction of Ca^{2+} entry in single nerve terminals. *Journal of Biological Chemistry*
814 277

815 Mineur YS, Huynh LX & Crusio WE (2006) Social behavior deficits in the Fmr1 mutant mouse.
816 *Behavioural Brain Research* 168

817 Mitsukawa K, Yamamoto R, Ofner S, Nozulak J, Pescott O, Lukic S, Stoehr N, Mombereau C,
818 Kuhn R, McAllister KH, *et al* (2005) A selective metabotropic glutamate receptor 7 agonist:
819 Activation of receptor signaling via an allosteric site modulates stress parameters in vivo.
820 *Proc Natl Acad Sci U S A* 102

821 Monday HR, Kharod SC, Yoon YJ, Singer RH & Castillo PE (2022) Presynaptic FMRP and
822 local protein synthesis support structural and functional plasticity of glutamatergic axon
823 terminals. *Neuron* 110

824 Nair JD, Henley JM & Wilkinson KA (2021) Surface biotinylation of primary neurons to
825 monitor changes in AMPA receptor surface expression in response to kainate receptor
826 stimulation. *STAR Protoc* 2

827 Di Nardo A, Kramvis I, Cho N, Sadowski A, Meikle L, Kwiatkowski DJ & Sahin M (2009)
828 Tuberous sclerosis complex activity is required to control neuronal stress responses in an
829 mTOR-dependent manner. *Journal of Neuroscience* 29

830 Niere F, Wilkerson JR & Huber KM (2012) Evidence for a fragile X mental retardation protein-
831 mediated translational switch in metabotropic glutamate receptor-triggered Arc translation
832 and long-term depression. *Journal of Neuroscience* 32

833 Ohishi H, Akazawa C, Shigemoto R, Nakanishi S & Mizuno N (1995) Distributions of the
834 mRNAs for L-2-amino-4-phosphonobutyrate-sensitive metabotropic glutamate receptors,
835 mGluR4 and mGluR7, in the rat brain. *Journal of Comparative Neurology* 360

836 Osterweil EK, Krueger DD, Reinhold K & Bear MF (2010) Hypersensitivity to mGluR5 and
837 ERK1/2 leads to excessive protein synthesis in the hippocampus of a mouse model of
838 fragile X syndrome. *Journal of Neuroscience* 30

839 Palazzo E, Marabese I, de Novellis V, Rossi F & Maione S (2016) Metabotropic Glutamate
840 Receptor 7: From Synaptic Function to Therapeutic Implications. *Curr Neuropharmacol* 14

841 Parveen S, Parthasarathy H, Vedagiri D, Gupta D, Nair G & Harinivas Harshan K (2021)
842 Regulation of eIF2 α Phosphorylation by MAPKs Influences Polysome Stability and 1
843 Protein Translation 2 3. <https://doi.org/10.1101/20210830458160>

844 Pyronnet S, Imataka H, Gingras AC, Fukunaga R, Hunter T & Sonenberg N (1999) Human
845 eukaryotic translation initiation factor 4G (eIF4G) recruits Mnk1 to phosphorylate eIF4E.
846 *EMBO Journal* 18

847 Raj N, McEachin ZT, Harousseau W, Zhou Y, Zhang F, Merritt-Garza ME, Taliaferro JM,
848 Kalinowska M, Marro SG, Hales CM, *et al* (2021) Cell-type-specific profiling of human
849 cellular models of fragile X syndrome reveal PI3K-dependent defects in translation and
850 neurogenesis. *Cell Rep* 35

851 Ronesi JA, Collins KA, Hays SA, Tsai NP, Guo W, Birnbaum SG, Hu JH, Worley PF, Gibson
852 JR & Huber KM (2012) Disrupted Homer scaffolds mediate abnormal mGluR5 function in
853 a mouse model of fragile X syndrome. *Nat Neurosci* 15: 431–440, s1

854 Rosenheck M, Sheeler C, Saré RM, Gurney ME & Smith CB (2021) Effects of chronic inhibition
855 of phosphodiesterase-4D on behavior and regional rates of cerebral protein synthesis in a
856 mouse model of fragile X syndrome. *Neurobiol Dis* 159

857 Sansig G, Bushell TJ, Clarke VRJ, Rozov A, Burnashev N, Portet C, Gasparini F, Schmutz M,
858 Klebs K, Shigemoto R, *et al* (2001) Increased seizure susceptibility in mice lacking
859 metabotropic glutamate receptor 7. *Journal of Neuroscience* 21

860 Santini E, Huynh TN, Longo F, Koo SY, Mojica E, D’Andrea L, Bagni C & Klann E (2017)
861 Reducing eIF4E-eIF4G interactions restores the balance between protein synthesis and actin
862 dynamics in fragile X syndrome model mice. *Sci Signal* 10

863 Saré RM, Levine M & Smith CB (2016) Behavioral phenotype of Fmr1 knock-out mice during
864 active phase in an altered light/dark cycle. *eNeuro* 3

865 Scharf SH, Jaeschke G, Wettstein JG & Lindemann L (2015) Metabotropic glutamate receptor 5
866 as drug target for Fragile X syndrome. *Curr Opin Pharmacol* 20
867 doi:10.1016/j.coph.2014.11.004 [PREPRINT]

868 Sethna F, Feng W, Ding Q, Robison AJ, Feng Y & Wang H (2017) Enhanced expression of
869 ADCY1 underlies aberrant neuronal signalling and behaviour in a syndromic autism model.
870 *Nat Commun* 8

871 Sharma A, Hoeffler CA, Takayasu Y, Miyawaki T, McBride SM, Klann E & Suzanne Zukin R
872 (2010) Dysregulation of mTOR signaling in fragile X syndrome. *Journal of Neuroscience*
873 30

874 Shigemoto R, Kinoshita A, Wada E, Nomura S, Ohishi H, Takada M, Flor PJ, Neki A, Abe T,
875 Nakanishi S, *et al* (1997) Differential presynaptic localization of metabotropic glutamate
876 receptor subtypes in the rat hippocampus. *Journal of Neuroscience* 17

877 Smith GD, White J & Lugo JN (2016) Superimposing Status Epilepticus on Neuron Subset-
878 Specific PTEN Haploinsufficient and Wild Type Mice Results in Long-term Changes in
879 Behavior. *Sci Rep* 6

880 Soden ME & Chen L (2010) Fragile X protein FMRP is required for homeostatic plasticity and
881 regulation of synaptic strength by retinoic acid. *Journal of Neuroscience* 30

882 Sukoff Rizzo SJ, Leonard SK, Gilbert A, Dollings P, Smith DL, Zhang MY, Di L, Platt BJ, Neal
883 S, Dwyer JM, *et al* (2011) The metabotropic glutamate receptor 7 allosteric modulator

884 AMN082: A monoaminergic agent in disguise? *Journal of Pharmacology and Experimental*
885 *Therapeutics* 338: 345–352

886 Tian Y, Yang C, Shang S, Cai Y, Deng X, Zhang J, Shao F, Zhu D, Liu Y, Chen G, *et al* (2017)
887 Loss of FMRP impaired hippocampal long-term plasticity and spatial learning in rats. *Front*
888 *Mol Neurosci* 10

889 Till SM, Asiminas A, Jackson AD, Katsanevaki D, Barnes SA, Osterweil EK, Bear MF,
890 Chattarji S, Wood ER, Wyllie DJA, *et al* (2015) Conserved hippocampal cellular
891 pathophysiology but distinct behavioural deficits in a new rat model of FXS. *Hum Mol*
892 *Genet* 24

893 Tsai NP, Wilkerson JR, Guo W, Maksimova MA, DeMartino GN, Cowan CW & Huber KM
894 (2012) Multiple autism-linked genes mediate synapse elimination via proteasomal
895 degradation of a synaptic scaffold PSD-95. *Cell* 151: 1581–1594

896 Turner G, Webb T, Wake S & Robinson H (1996) Prevalence of fragile X syndrome. *Am J Med*
897 *Genet* 64

898 Waskiewicz AJ, Flynn A, Proud CG & Cooper JA (1997) Mitogen-activated protein kinases
899 activate the serine/threonine kinases Mnk1 and Mnk2. *EMBO Journal* 16

900 Xie J, Ponuwei GA, Moore CE, Willars GB, Tee AR & Herbert TP (2011) CAMP inhibits
901 mammalian target of rapamycin complex-1 and -2 (mTORC1 and 2) by promoting complex
902 dissociation and inhibiting mTOR kinase activity. *Cell Signal* 23

903 Yang Y & Pan C (2013) Role of metabotropic glutamate receptor 7 in autism spectrum disorders:
904 A pilot study. *Life Sci* 92

905

906

907

908

909 **FIGURE LEGENDS**

910 **Figure 1. Activation of mGluR7 reduces protein synthesis in both WT and *Fmr1* KO**
911 **neurons.**

912 (A) Representative fluorescence images showing expression of mGluR7a in CA1, CA3 and
913 dentate gyrus (DG) in brain sections obtained from WT, *Fmr1* KO and *mGluR7* KO mice at
914 postnatal (P) day 60.

915 (B) Representative western blots and quantification showing the expression of mGluR7a and
916 mGluR7b in total brain lysate from WT and *Fmr1* KO mice at P60. (n = 4 mice; p = 0.8946 and
917 0.3038 for mGluR7a and mGluR7b, respectively)

918 (C) Representative western blots and quantification of mGluR7a, mGluR7b and surface protein
919 marker N-Cadherin from total cell lysates or extracted surface protein fractions in primary
920 cortical neuron cultures made from WT or *Fmr1* KO mice (n = 6 independent cultures; p =
921 0.0387 and 0.0463 for mGluR7a and mGluR7b, respectively).

922 (D) Representative western blots and quantifications of puromycin and GAPDH from WT and
923 *Fmr1* KO cortical neuron cultures at DIV 12-14 treated with DMSO, AMN082 (1 μ M) or
924 MMPIP (1 μ M) for 1 hour followed by treatment of puromycin (10 μ g/ml) to label newly
925 synthesized protein for another hour. (n = 5 and 3 for WT and *Fmr1* KO, respectively)
926 (WT+DMSO vs WT+AMN082, p = 0.0285; WT+DMSO vs WT+MMPIP, p = 0.9141;
927 WT+DMSO vs *Fmr1*KO+DMSO, p < 0.0001; *Fmr1*KO+DMSO vs *Fmr1*KO+AMN082, p <
928 0.0001; *Fmr1*KO+DMSO vs *Fmr1*KO+MMPIP, p = 0.3435).

929 (E) Representative western blots and quantifications of puromycin and GAPDH from WT or
930 *mGluR7* KO cortical neuron cultures at DIV 12-14 treated with DMSO, AMN082 (1 μ M) or
931 MMPIP (1 μ M) for 1 hour followed by treatment of puromycin (10 μ g/ml). A set of blots
932 showing the levels of mGluR7a and mGluR7b in WT and *mGluR7* KO cultures is on the right. (n
933 = 4) (DMSO vs AMN082, p = 0.732; DMSO vs MMPIP, p = 0.6935)

934 (F, G, H, I) Representative western blots and quantifications of ERK1/2 phosphorylation, mTOR
935 phosphorylation, eIF4E phosphorylation and eIF2 α phosphorylation from WT and *Fmr1* KO
936 cortical neuron cultures at DIV 12-14 treated with DMSO or AMN082 (1 μ M) for 1 hour. For
937 the quantification, phosphorylation signal of a specific protein was normalized to its total protein
938 signal. (n = 3-5 independent cultures) (F: WT+DMSO vs WT+AMN082, p = 0.0339;
939 WT+DMSO vs *Fmr1*KO+DMSO, p = 0.0017; *Fmr1*KO+DMSO vs *Fmr1*KO+AMN082, p <
940 0.0001. G: WT+DMSO vs WT+AMN082, p = 0.9571; WT+DMSO vs *Fmr1*KO+DMSO, p =
941 0.4032; *Fmr1*KO+DMSO vs *Fmr1*KO+AMN082, p = 0.7514. H: WT+DMSO vs WT+AMN082,
942 p = 0.0074; WT+DMSO vs *Fmr1*KO+DMSO, p = 0.8646; *Fmr1*KO+DMSO vs
943 *Fmr1*KO+AMN082, p = 0.0005. I: WT+DMSO vs WT+AMN082, p = 0.7174; WT+DMSO vs
944 *Fmr1*KO+DMSO, p = 0.8258; *Fmr1*KO+DMSO vs *Fmr1*KO+AMN082, p = 0.4377)

945 (J) Representative western blots and quantification of eIF4E and eIF4G pulled down by m7GTP
946 beads from WT and *Fmr1* KO cortical neuron cultures treated with DMSO or AMN082 (1 μ M)
947 at DIV 12-14. (n = 4 independent cultures) (WT+DMSO vs WT+AMN082, p = 0.0249;
948 WT+DMSO vs *Fmr1*KO+DMSO, p = 0.7503; *Fmr1*KO+DMSO vs *Fmr1*KO+AMN082, p =
949 0.0038)

950 Data Information: Data were analyzed by Student's *t*-test (B, C), one-way ANOVA (E) or two-
951 way ANOVA (D, F, G, H, I, and J) with Tukey test and presented as mean \pm SEM with **p* <
952 0.05, ***p* < 0.01, ****p* < 0.001, *****p* < 0.0001 and NS: non-significant.

953

954 **Figure 2. mGluR7 activation represses protein synthesis and phosphorylation of ERK1/2**
955 **and eIF4E in WT and *Fmr1* KO mouse hippocampus.**

956 (A) Representative western blots (left) and quantification (right) of puromycin and GAPDH in
957 the hippocampus of 6-8 weeks old WT and *Fmr1* KO mouse injected with saline or AMN082 (1
958 mg/kg) and puromycin (200 mg/kg) for one hour. (n = 4 mice per treatment group) (WT+Saline
959 vs WT+AMN082, p = 0.0463; WT+Saline vs *Fmr1*KO+Saline, p = 0.0135; *Fmr1*KO+Saline vs
960 *Fmr1*KO+AMN082, p = 0.0042)

961 (B) Representative western blots of puromycin and GAPDH in the hippocampus of *mGluR7* KO
962 mice injected with saline or AMN082 (1 mg/kg) and puromycin (200 mg/kg) for one hour. (n = 4
963 mice per treatment group; p = 0.3206).

964 (C and D) Left: representative western blots of p-ERK1/2 and p-eIF4E in hippocampal lysates
965 from WT and *Fmr1* KO mice treated with AMN082 (1 mg/kg) for one hour (on left) and the
966 quantification (on right) showing phosphorylated protein levels normalized to their respective
967 total protein levels. (n = 5 mice) (C: WT+Saline vs WT+AMN082, p = 0.0044; WT+Saline vs
968 *Fmr1*KO+Saline, p < 0.0001; *Fmr1*KO+Saline vs *Fmr1*KO+AMN082, p < 0.0001. D:
969 WT+Saline vs WT+AMN082, p = 0.0028; WT+Saline vs *Fmr1*KO+Saline, p = 0.9998;
970 *Fmr1*KO+Saline vs *Fmr1*KO+AMN082, p = 0.0451)

971 (E) The schematic showing the signaling pathway implicated in the reduction of protein
972 synthesis following the activation of mGluR7.

973 Data Information: Data were analyzed by Student's *t*-test (B) or two-way ANOVA with Tukey
974 test (A, C, D) and presented as mean ± SEM with **p* < 0.05, ***p* < 0.01, *****p* < 0.0001 and NS:
975 non-significant.

976

977 **Figure 3. Activation of mGluR7 reduces neuronal excitability and susceptibility to**
978 **audiogenic seizure in *Fmr1* KO mice.**

979 (A) Representative raster plots of spontaneous spikes from WT (top) and *Fmr1* (bottom) cortical
980 neuron cultures treated with DMSO, AMN082 (1 μ M) or MMPIP (1 μ M) for 1 hour at DIV 12-
981 14. Quantification of burst duration, burst frequency and average number of spikes by comparing
982 “after treatment” to “before treatment”, from the same culture was shown on the right. (n = 5
983 independent cultures). (WT, Burst Duration: DMSO vs AMN082, $p < 0.0001$; DMSO vs MMPIP,
984 $p = 0.9924$; Burst Frequency: DMSO vs AMN082, $p < 0.0001$; DMSO vs MMPIP, $p = 0.4762$;
985 Average number of spikes: DMSO vs AMN082, $p < 0.0001$; DMSO vs MMPIP, $p = 0.1294$.
986 *Fmr1* KO: Burst Duration: DMSO vs AMN082, $p < 0.0001$; DMSO vs MMPIP, $p = 0.1751$;
987 Burst Frequency: DMSO vs AMN082, $p < 0.0001$; DMSO vs MMPIP, $p = 0.5922$; Average
988 number of spikes: DMSO vs AMN082, $p < 0.0001$; DMSO vs MMPIP, $p = 0.8932$)

989 (B) Left: Representative traces of action potentials induced by 200 pA from wild-type (top) or
990 *Fmr1* KO (bottom) cortical neurons treated with DMSO or AMN082 (1 μ M) for 1 hour. Right:
991 Average action potential firing rates (Hz) evoked by 0–200 pA injection from wild-type (top) or
992 *Fmr1* KO (bottom) neurons treated with DMSO or AMN082 (1 μ M). (n = 12-14 neurons per
993 treatment group) (WT: p values for current stimulations between 140 pA and 200 pA are 0.0477,
994 0.0335, 0.0438, 0.0424, 0.0359, 0.0317 and 0.0348. *Fmr1* KO: p values for current stimulations
995 between 140 pA and 200 pA are 0.0314, 0.0319, 0.0494, 0.0287, 0.0450, 0.0245 and 0.0266)

996 (C) A schematic showing the experimental design for audiogenic seizure in *Fmr1* KO mice (top).
997 Quantification of seizure scores after *Fmr1* KO mice were injected with saline or AMN082 (1
998 mg/kg) for 30 minutes. (n = 6 per treatment group; $p = 0.0281$).

999 Data Information: Data were analyzed by one-way ANOVA with Tukey test (A, B) or two-tailed
1000 Mann Whitney test (C) and presented as mean \pm SEM with * $p < 0.05$, **** $p < 0.0001$ and NS:
1001 non-significant.

1002

1003 **Figure 4. Activation of mGluR7 ameliorates repetitive behavior without affecting**
1004 **locomotor activity or sociability in *Fmr1* KO mice.**

1005 (A) Representative images of the marbles' configuration before and after allowing mice to bury
1006 marbles for 30 minutes (left). WT or *Fmr1* KO mice were intraperitoneally injected with saline
1007 or AMN082 (1 mg/kg) for 1 hour before the test. Quantification of the marble burying activity is
1008 shown on the right. (n = 10 mice per treatment group) (WT+Saline vs WT+AMN082, $p = 0.9791$;
1009 WT+Saline vs *Fmr1*KO+Saline, $p = 0.0004$; *Fmr1*KO+Saline vs *Fmr1*KO+AMN082, $p =$
1010 0.0008.)

1011 (B) Representative traces from a 5-minute test period in an open-field arena (left) showing the
1012 movement of WT or *Fmr1* KO mice after intraperitoneally injected with saline or AMN082 (1
1013 mg/kg) for 1 hour. Quantification of total distance traveled, immobile time and time spent in
1014 central zone is shown on the right. (n = 10 mice per treatment group) (Distance traveled:
1015 WT+Saline vs WT+AMN082, $p = 0.9961$; WT+Saline vs *Fmr1*KO+Saline, $p = 0.1124$;
1016 *Fmr1*KO+Saline vs *Fmr1*KO+AMN082, $p = 0.5765$. Immobile time: WT+Saline vs
1017 WT+AMN082, $p = 0.8525$; WT+Saline vs *Fmr1*KO+Saline, $p = 0.1211$; *Fmr1*KO+Saline vs
1018 *Fmr1*KO+AMN082, $p = 0.9636$. Time in zone: WT+Saline vs WT+AMN082, $p = 0.6004$;
1019 WT+Saline vs *Fmr1*KO+Saline, $p = 0.0482$; *Fmr1*KO+Saline vs *Fmr1*KO+AMN082, $p =$
1020 0.9786)

1021 (C) The three-chamber social interaction test from WT or *Fmr1* KO mice after intraperitoneally
1022 injected with saline or AMN082 (1 mg/kg) for 1 hour. Schematic representation depicting the
1023 sociability protocol for the three-chamber social interaction test was also shown. (n = 10 mice
1024 per treatment group) (WT+Saline, $p < 0.0001$; WT+AMN082, $p < 0.0001$, *Fmr1*KO+Saline, $p =$
1025 0.0009 , and *Fmr1*KO+AMN082, $p < 0.0001$)

1026 Data Information: Data were analyzed by two-way ANOVA with Tukey's or Šidák's test and
1027 presented as mean \pm SEM with * $p < 0.05$, ** $p < 0.01$, *** $p < 0.001$ and NS: non-significant.

1028

1029 **Figure 5. Activation of mGluR7 improves learning and memory in *Fmr1* KO mice.**

1030 (A) A schematic showing the novel object recognition test paradigm (top) and the quantification
1031 of preference index from WT or *Fmr1* KO mice after intraperitoneally injected with saline or
1032 AMN082 (1 mg/kg) for 1 hour (bottom). (n = 10 mice per treatment group) (WT+Saline vs
1033 WT+AMN082, $p = 0.9999$; WT+Saline vs *Fmr1*KO+Saline, $p = 0.0008$; *Fmr1*KO+Saline vs
1034 *Fmr1*KO+AMN082, $p = 0.0002$)

1035 (B) A schematic depiction of contextual fear conditioning test paradigm (top) and quantification
1036 of the freezing behavior of WT or *Fmr1* KO mice after intraperitoneally injected with saline or
1037 AMN082 (1 mg/kg) for 1 hour (bottom). (n = 10 mice per treatment group) (In Shock groups:
1038 WT+Saline vs WT+AMN082, $p = 0.1642$; WT+Saline vs *Fmr1*KO+Saline, $p = 0.0066$;
1039 *Fmr1*KO+Saline vs *Fmr1*KO+AMN082, $p = 0.418$)

1040 (C) A schematic representation of Barnes maze test showing the training trail and probe trial.
1041 WT or *Fmr1* KO mice intraperitoneally injected with saline or AMN082 (1 mg/kg) were trained
1042 for 4 days with 3 consecutive trials every day to locate the escape box (green circle). The escape

1043 latency and number of errors during the training trial were quantified. Quadrant occupancy on
1044 probe trial on day 5 was assessed by recording the time spent in the target area (yellow area). (n
1045 = 10 mice per treatment group) (Escape latency, Day 1: WT+Saline vs WT+AMN082, p =
1046 0.9999; WT+Saline vs *Fmr1*KO+Saline, p = 0.9999; *Fmr1*KO+Saline vs *Fmr1*KO+AMN082, p
1047 = 0.9999; Day 2: WT+Saline vs WT+AMN082, p = 0.9999; WT+Saline vs *Fmr1*KO+Saline, p =
1048 0.9999; *Fmr1*KO+Saline vs *Fmr1*KO+AMN082, p = 0.9999; Day 3: WT+Saline vs
1049 WT+AMN082, p = 0.9999; WT+Saline vs *Fmr1*KO+Saline, p = 0.4132; *Fmr1*KO+Saline vs
1050 *Fmr1*KO+AMN082, p = 0.3069; Day 1: WT+Saline vs WT+AMN082, p = 0.9999; WT+Saline
1051 vs *Fmr1*KO+Saline, p = 0.9953; *Fmr1*KO+Saline vs *Fmr1*KO+AMN082, p = 0.7988. Number
1052 of errors, Day 1: WT+Saline vs WT+AMN082, p = 0.9999; WT+Saline vs *Fmr1*KO+Saline, p =
1053 0.9999; *Fmr1*KO+Saline vs *Fmr1*KO+AMN082, p = 0.9999; Day 2: WT+Saline vs
1054 WT+AMN082, p = 0.9999; WT+Saline vs *Fmr1*KO+Saline, p = 0.8944; *Fmr1*KO+Saline vs
1055 *Fmr1*KO+AMN082, p = 0.9999; Day 3: WT+Saline vs WT+AMN082, p = 0.9999; WT+Saline
1056 vs *Fmr1*KO+Saline, p = 0.9999; *Fmr1*KO+Saline vs *Fmr1*KO+AMN082, p = 0.4095; Day 4:
1057 WT+Saline vs WT+AMN082, p = 0.9999; WT+Saline vs *Fmr1*KO+Saline, p = 0.9999;
1058 *Fmr1*KO+Saline vs *Fmr1*KO+AMN082, p = 0.9999. Quadrant occupancy: WT+Saline vs
1059 WT+AMN082, p = 0.0676; WT+Saline vs *Fmr1*KO+Saline, p = 0.8267; *Fmr1*KO+Saline vs
1060 *Fmr1*KO+AMN082, p = 0.9493)

1061 Data Information: Data were analyzed by two-way ANOVA with Tukey's test and presented as
1062 mean \pm SEM with * $p < 0.05$, ** $p < 0.01$, *** $p < 0.001$ and NS: non-significant.

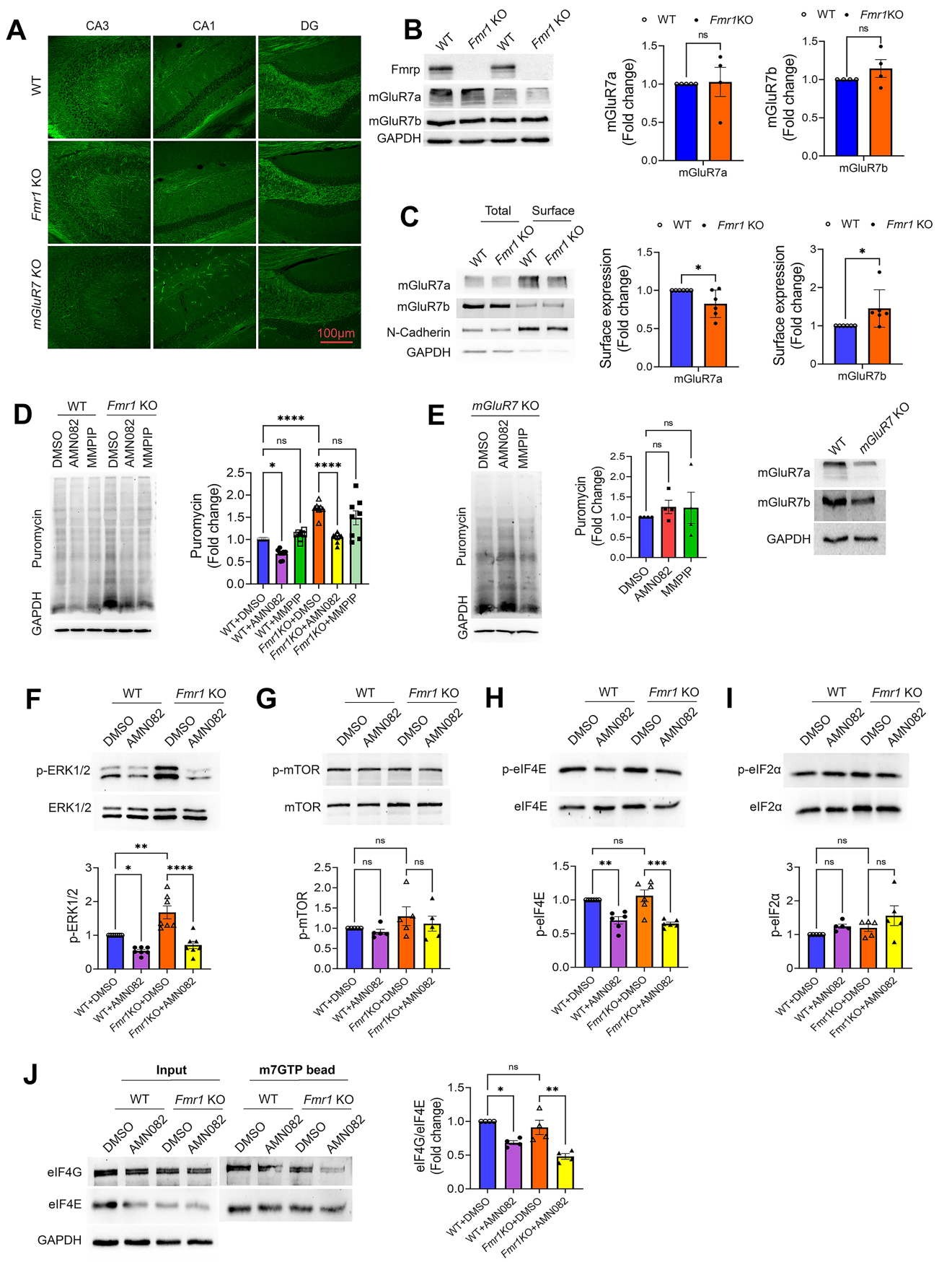
1063 **(D)** Summary of the effects from activation of mGluR7 on molecular and behavioral deficits in
1064 *Fmr1* KO mice.

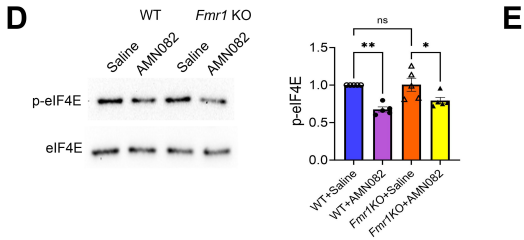
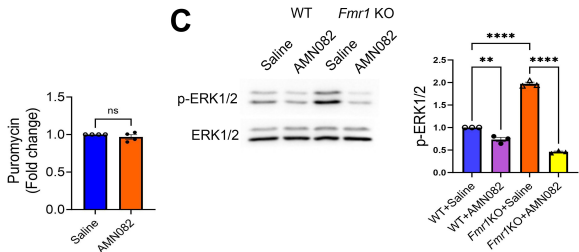
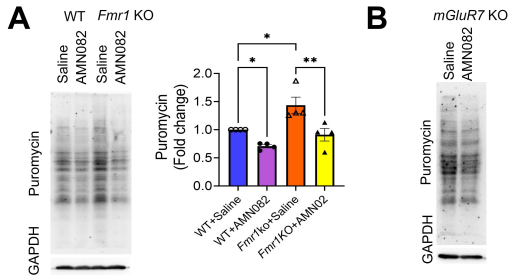
1065

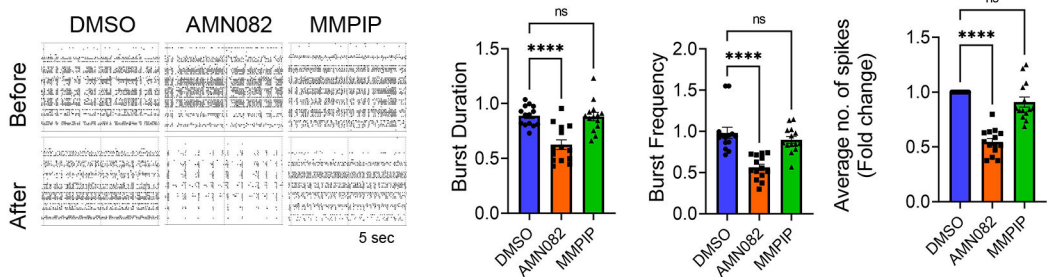
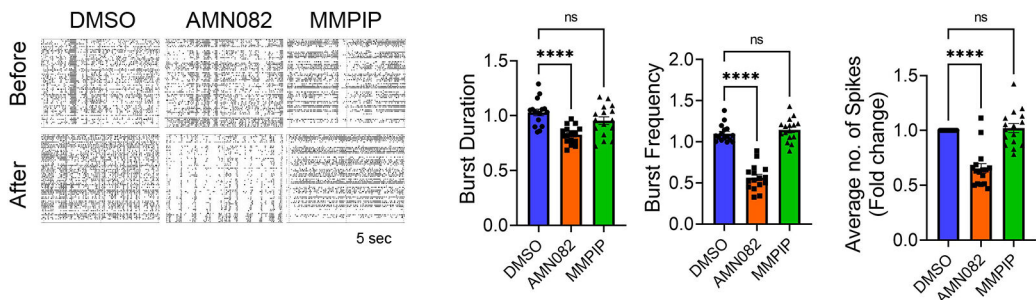
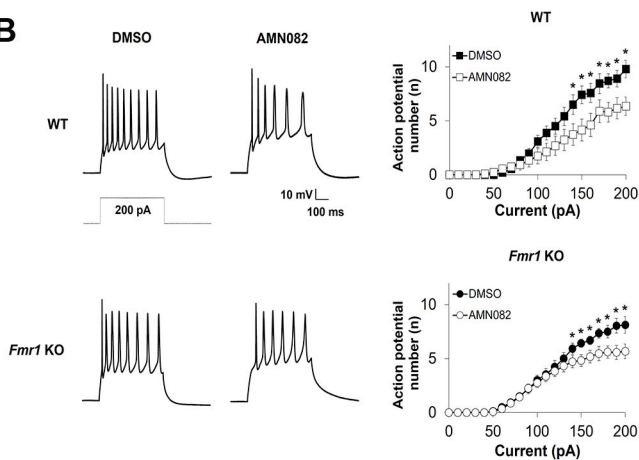
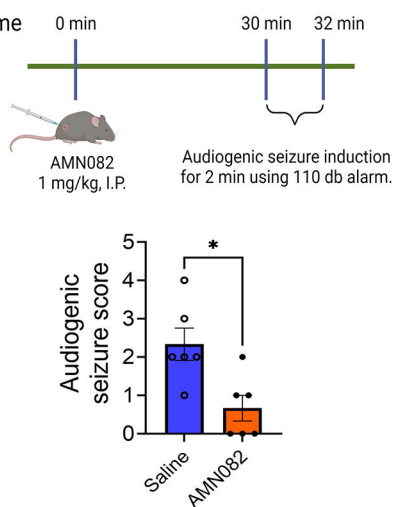
1066 **EXPANDED VIEW FIGURE LEGENDS**

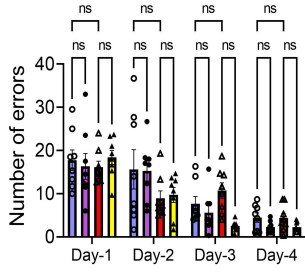
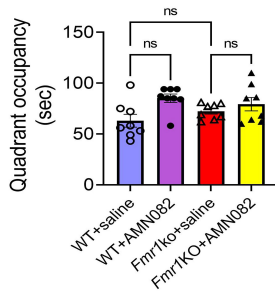
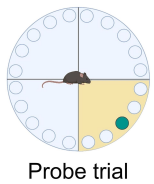
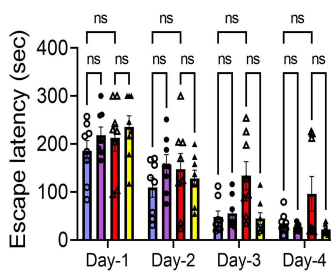
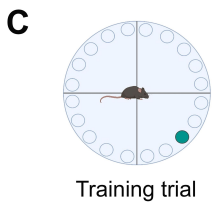
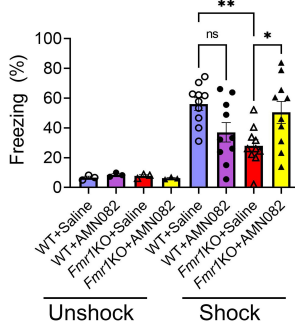
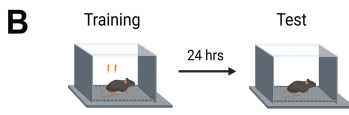
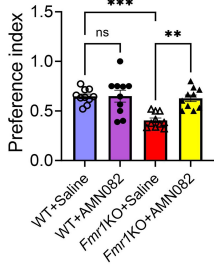
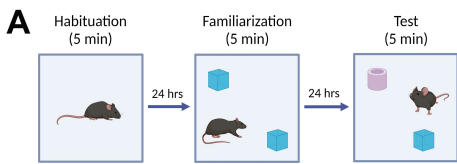
1067 **Figure EV1. Activation of mGluR reduced the levels of an Fmrp target protein Pcdh7 in**
1068 **the WT and *Fmr1* KO hippocampus.** Top: Representative blot showing expression of Pcdh7 in
1069 the hippocampal lysates of 6-8 weeks old WT and *Fmr1* KO mice injected with saline or
1070 AMN082 (1 mg/kg). Bottom: Plot showing the quantification of band intensities of Pcdh7 from 4
1071 independent sets of experiments expressed as fold change. Data were analyzed using Two-way
1072 ANOVA with Tukey's test and presented as mean +/- SEM. WT+Saline vs WT+AMN082, p =
1073 0.0213; WT+Saline vs *Fmr1*KO+Saline, p = 0.0120; *Fmr1*KO+Saline vs *Fmr1*KO+AMN082, p
1074 = 0.0021

1075



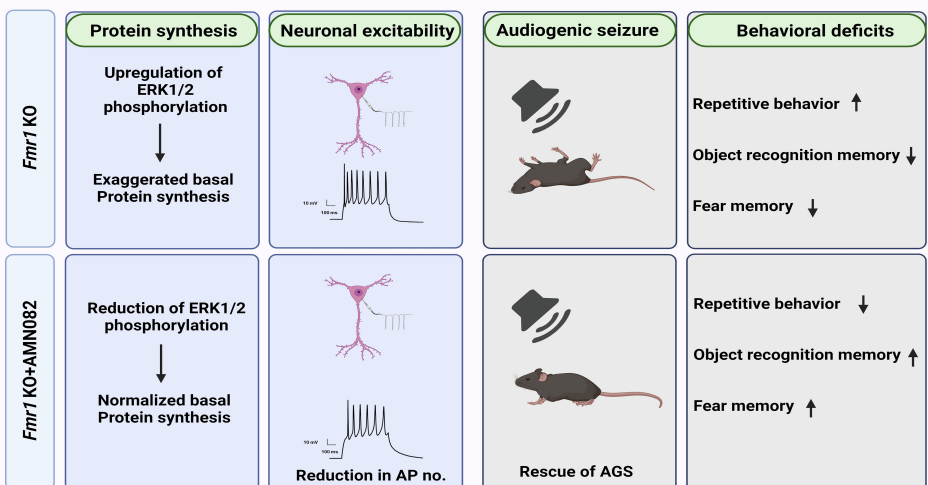


A WT*Fmr1* KO**B****C**



- WT+Saline
- WT+AMN082
- ▲ Fmr1KO+Saline
- ▲ Fmr1KO+AMN082

D



WT

Fmr1 KO

Saline

AMN082

Saline

AMN082

Pcdh7



GAPDH

